Solar Phys (2010) 264: 119–147
DOI 10.1007/s11207-010-9558-8

Revealing the Fine Structure of Coronal Dimmings and Associated Flows with *Hinode*/EIS

Implications for Understanding the Source Regions of Sustained Outflow Following CMEs

G.D.R. Attrill · L.K. Harra · L. van Driel-Gesztelyi · M.J. Wills-Davey

Received: 8 February 2010 / Accepted: 8 April 2010 / Published online: 24 April 2010

Abstract We study two CME events on 13 and 14 December 2006 that were associated with large-scale dimmings. We study the eruptions from pre-event on 11 December through the recovery on 15 December, using a combination of *Hinode*/EIS, SOHO/EIT, SOHO/MDI, and MLSO Hα data. The GOES X-class flares obscured the core dimmings, but secondary dimmings developed remote from the active region (AR) in both events. The secondary dimmings are found to be formed by a removal of bright coronal material from loops in the plage region to the East of the AR. Using *Hinode*/EIS data, we find that the outflows associated with the coronal-dimming regions are highly structured. The concentrated outflows are located at the footpoints of coronal loops (which exist before, and are re-established after, the eruptions), and these are correlated with regions of positive magnetic elements. Comparative study of the *Hinode*/EIS and SOHO/EIT data shows that the reduction in outflow velocity is consistent with the recovery in intensity of the studied regions. We find that concentrated downflows develop during the recovery phase of the dimmings and are also correlated with the same positive magnetic elements that were previously related to outflows.

The local behaviour of the flows in and around the dimming regions following the eruptions is found to be dynamic and complex. Despite the global aspects of these events (wide-

Electronic supplementary material The online version of this article (doi:10.1007/s11207-010-9558-8) contains supplementary material, which is available to authorized users.

G.D.R. Attrill (✉) · M.J. Wills-Davey
Harvard-Smithsonian Center for Astrophysics, 60 Garden Street, Cambridge, MA 02138, USA
e-mail: gattrill@cfa.harvard.edu

L.K. Harra · L. van Driel-Gesztelyi
UCL-Mullard Space Science Laboratory, Holmbury St. Mary, Dorking, Surrey RH5 6NT, UK

L. van Driel-Gesztelyi
Observatoire de Paris, LESIA, UMR 8109, CNRS, 92195 Meudon Principal Cedex, France

L. van Driel-Gesztelyi
Konkoly Observatory of the Hungarian Academy of Sciences, Budapest, Hungary

spread dimmings, CMEs, coronal waves) being largely homologous, there are significant local variations and distinct differences between the flows associated with the two events. We find that the secondary dimmings recover primarily by re-establishment of the bright coronal loops (the exact configuration changes between the eruptions, which is reflected by the complexity of the flows).

1. Introduction

1.1. Coronal Dimmings

Coronal dimmings are usually observed as decreases in intensity in soft X-rays (Hudson, Acton, and Freeland, 1996; Sterling and Hudson, 1997) and extreme ultra-violet (EUV) data (Thompson *et al.*, 1998). They appear relatively suddenly, on timescales of minutes. There are two generally accepted possibilities that can cause coronal dimming:

i) A density depletion caused by an evacuation of plasma (Hudson, Acton, and Freeland, 1996). Such an effect may be caused by the eruption of the local magnetic field, leading to considerable expansion of magnetic loops into interplanetary space. The expansion creates a larger volume, leading to a region of decreased plasma density.

ii) A change in temperature (see, *e.g.*, Thompson *et al.*, 1998; Chertok and Grechnev, 2003). Differences observed between images in different emission lines suggest that some secondary temperature variations may also be responsible for the appearance of dimmings. However, Hudson, Acton, and Freeland (1996) showed that the timescale of the dimming formation observed in *Yohkoh*/SXT data is much faster than corresponding conductive and radiative cooling times, which suggests that the dimmings are primarily a result of density depletion rather than a temperature effect.

1.2. Association with CMEs

During a coronal mass ejection (CME), the plasma density may be depleted as a result of evacuation caused by the significant expansion of the magnetic field. Upon eruption of the flux-rope (which makes up the core field of the associated CME), the magnetic loops rooted in the dimming regions greatly expand to heights much larger than the gravitational scale height of the plasma. As a result, the plasma can escape the corona and the dimming regions are believed to exhibit a decrease in intensity as the plasma is evacuated along the "open" field lines (Thompson *et al.*, 2000). Measurement of plasma Doppler motions in coronal-dimming regions using SOHO/CDS data (Harrison and Lyons, 2000; Harra and Sterling, 2001) and more recently with *Hinode*/EIS (Harra *et al.*, 2007; Imada *et al.*, 2007; Jin *et al.*, 2009), has shown that blueshifted motions indeed indicate plasma outflow from coronal dimmings. The blue-shifted flows are understood to be a consequence of the change in the magnetic field from a closed to an "open" (greatly expanded) configuration.

Although coronal dimming has been closely associated with CMEs since the 1970s (see, *e.g.*, Rust and Hildner, 1976) and dimmings are now widely acknowledged as an indicator of front-side CMEs (see, *e.g.*, Thompson *et al.*, 2000; Hudson and Cliver, 2001), the CME-dimming association was only confirmed recently using statistical analysis (Bewsher, Harrison, and Brown, 2008; Reinard and Biesecker, 2008). In classical "double dimming" events (*e.g.* 7 April 1997, 12 May 1997), coronal dimmings are understood to mark the position of the footpoints of an erupted flux-rope that makes up the core magnetic field of the

associated CME (Hudson and Webb, 1997; Sterling and Hudson, 1997; Webb *et al.*, 2000; Mandrini *et al.*, 2005).

Whilst we acknowledge that coronal dimmings can be reasonably confidently linked to the occurrence of a CME, the absence of coronal dimmings does not preclude the onset of a CME. Recent work by Robbrecht, Patsourakos, and Vourlidas (2009) and Ma *et al.* (2010) using STEREO data has shown that slow-rise CMEs (that originate from high in the corona and are associated with weak magnetic fields) may not remove material from the low corona at a detectable level. In such cases, coronal dimming may be absent even for spatially large CMEs.

1.3. Secondary Dimmings

In global-scale events occurring in complex ARs, the spatial organisation of the dimmings can be complicated. Secondary dimmings can develop remote from the initial source region, and their involvement in the eruption may not be as straightforward as for core dimmings (Attrill *et al.*, 2007; Mandrini *et al.*, 2007). Secondary dimmings were (to our knowledge) first reported in a study of seven CME events by Thompson *et al.* (2000). The weaker brightness depletions were found to be extended from the flare site and generally mapped out the apparent footprint of the associated CME. However, this study did not ascertain what the secondary dimmings actually are.

Another phenomenon that can occur in connection with CMEs and their associated dimmings are coronal waves (see, *e.g.*, Thompson *et al.*, 1998). There is much debate regarding the physical nature of coronal waves (see Warmuth, 2007; Vršnak and Cliver, 2008; Attrill, 2008; Wills-Davey and Attrill, 2010 for recent reviews), but it is well established both statistically (see, *e.g.*, Biesecker *et al.*, 2002; Cliver *et al.*, 2005) and via case-study analyses (see, *e.g.*, Veronig, Temmer, and Vršnak, 2008; Cohen *et al.*, 2009; Chen, 2009) that they are strongly associated with CMEs. If coronal waves are interpreted as fast-mode MHD waves, then coronal dimmings that are observed behind the expanding coronal wave front may be interpreted as rarefied regions that develop behind a freely propagating wavefront (*e.g.* as in Wu *et al.*, 2001), since a rarefaction shock develops at the trailing part of a large-amplitude perturbation (Landau and Lifshitz, 1987). However, this interpretation may not be sufficient to explain the secondary dimmings in some events, because dimmings formed by such a mechanism would be relatively short-lived, with a duration on Alfvén timescales (a few minutes), contrary to observations (see, *e.g.*, Cliver *et al.*, 2005; Delannée, Hochedez, and Aulanier, 2007; Mandrini *et al.*, 2007; Attrill *et al.*, 2009).

The relatively long lifetimes of secondary dimmings (on the order of hours), coupled with their mapping to the CME cavity (see, *e.g.*, Cohen *et al.*, 2009; Attrill *et al.*, 2009; Chen, 2009), strongly suggests that like the core dimmings, which persist on the order of days, secondary dimmings are also due to plasma evacuation. The plasma is evacuated into the expanding CME either by direct expansion of the magnetic field rooted in the secondary dimming region, or via reconnection between the core CME and surrounding magnetic field (see, *e.g.*, Attrill *et al.*, 2007; Mandrini *et al.*, 2007; Cohen *et al.*, 2009). The existence of secondary dimmings for any given event therefore depends on the extended magnetic connectivity that develops dynamically between the CME and surrounding magnetic structures during the eruption, which depends on the angular width of the CME. Narrow CME eruptions are restricted to disturbing a single active region, and the eruption often proceeds purely radially (as per the standard model for solar eruptions). However, when there is a significant lateral component to the CME expansion, so that the CME interacts with the surrounding magnetic field, secondary dimmings are expected to occur – reflecting the response of the global corona to the CME. Van Driel-Gesztelyi *et al.* (2008) discuss further

the importance of the surrounding magnetic topology for the development of low coronal signatures of CMEs.

1.4. Recovery of Coronal Dimmings

The recovery of coronal dimmings is a relatively new area of research. Kahler and Hudson (2001) studied 19 dimming events observed in *Yohkoh*/SXT (Tsuneta *et al.*, 1991) data and found that the dimmings tended to disappear by a net contraction of the boundaries rather than by brightening within the dimmings. They suggested that reconnection with "open" field of opposite polarity may occur with the "open" field at the outer boundaries of transient coronal holes without any signature of arcade formation. They specify that such "open" field lines may be found in previously existing coronal holes, open-field inclusions in the quiet-Sun corona, or in sunspot umbrae.

McIntosh *et al.* (2007) studied the post-eruptive evolution of the dimmings on 6 July 2006 using TRACE and SOHO/EIT data combined with MDI magnetograms. They report the reintroduction of moss spreading outward from the active region (AR) and interpret this as a consequence of the post-CME closure of the global coronal field above the AR following disconnection of the departed CME. McIntosh *et al.* (2007) find that the evolution of the dimmings are entirely dependent on the amount of unbalanced magnetic flux present in the AR following the CME and on how that flux is distributed. As the global coronal magnetic field closes from above by reconnection, following the "disconnection" of the CME, the plasma below no longer "feels" an open field above, and so the spicular ejecta become trapped (as before the eruption) and the energy balance returns to favour the thermal (over the kinetic) component. The dimmings begin to fill from beneath stochastically (hence the re-emergence of the moss), but with an enhanced rate in regions where unbalanced magnetic flux is available.

However, coronal dimmings often extend considerably far out into the quiet-Sun magnetic field (Webb *et al.*, 2000; Mandrini *et al.*, 2005; Attrill *et al.*, 2006), away from the AR and the domain where moss is observed (Berger *et al.*, 1999). Attrill *et al.* (2008) studied three such dimming events and suggested that rather than purely a *closure* of the global coronal magnetic field, interchange reconnections between the "open" magnetic field of the dimming, small coronal loops and emerging flux bipoles may act to *disperse* the concentration of "open" magnetic field forming the dimming out into the surrounding quiet Sun. In this picture, the intensity of the dimming is recovered whilst the magnetic connectivity to the Sun is maintained.

Jin *et al.* (2009) studied the coronal-dimming events on 13 and 14 December 2006 (the subjects of this work), and concluded that the recovery of the dimmings is primarily due to a replenishing mass supply that comes from the lower transition region, due to the dynamic response of the transition region to the enhanced pressure gradient as the CME eruption evacuates the plasma in the low corona.

1.5. Focus of This Work

Here, we study the flows associated with the 13 and 14 December 2006 dimmings, following the evolution from 11 December at 00:25 UT until 15 December at 11:12 UT in *Hinode*/EIS data. Figure 1 shows the location of the EIS field of view in the context of a SOHO/EIT image. We study the intensity change in the dimming regions using EIT data until 15:24 UT on 15 December. *Hinode*/XRT synoptic data are used to provide additional constraints from a global perspective. We additionally employ MLSO Hα and SOHO/MDI data to derive a

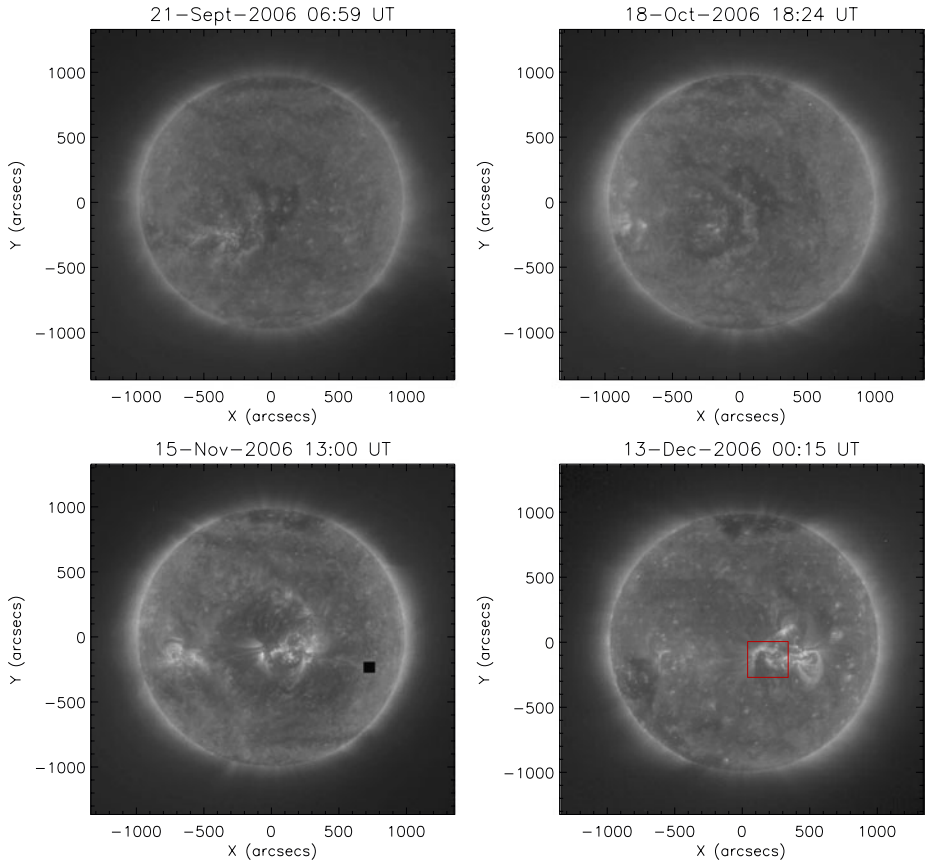

Figure 1 SOHO/EIT 171 Å logarithmically-scaled images for successive solar rotations (from September 2006) leading up to 00:15 UT on 13 December 2006. Active region NOAA 10930 developed in a region of reduced intensity. The red box in the bottom-right panel indicates the field of view for the corresponding *Hinode*/EIS observations, which focused on a plage region to the East of the active region.

multi-wavelength understanding of the activity associated with the formation and recovery of the coronal dimmings.

We find that the recovery of the coronal dimmings occurs (in both events) as a result of the reformation of relatively large-scale, overlying bright, coronal loops. This differs from the recovery mechanisms suggested by McIntosh *et al.* (2007), Attrill *et al.* (2008), and Jin *et al.* (2009) (discussed in Section 1.4), since these studies all suggest (to varying extents) that the coronal dimmings primarily refill from below.

The activity that occurred during this period in December 2006 has been the focus of several studies. Harra *et al.* (2009) analysed the changes in the AR using *Hinode*/EIS data from 9 – 13 December 2006. The coronal dimmings that formed during the two events on 13 and 14 December have been particularly studied, due to the fact that the region was well-observed by *Hinode*/EIS (*e.g.* Harra *et al.*, 2007; Imada *et al.*, 2007; Jin *et al.*, 2009; McIntosh, 2009). Existing work on these events is briefly reviewed in Section 2. We then describe the data used in this study in Section 3, before presenting our results in Section 4. Finally, we discuss the implications of our results in Section 5.

2. Overview of Previous Work on the Two Events

2.1. 13 December 2006 Event

AR NOAA 10930 (S06, W22) (from which both eruptions on 13 and 14 December originated), had a strong imbalance of magnetic flux. The AR was dominantly negative (Schrijver *et al.*, 2008), and "open" magnetic field was rooted in the negative-polarity sunspot. Due to the location of the AR in what had been a low-latitude coronal hole (Figure 1), an anemone-like structure developed, with large-scale coronal loops reaching from the surroundings into the negative-polarity sunspot.

At 02:54 UT, a halo CME eruption was recorded in the LASCO CME catalogue (Yashiro *et al.*, 2004). It was accompanied by a GOES X3.4-class flare that started at 02:14 UT in this AR (Kubo *et al.*, 2007), and a filament lying in the East – West direction (Williams *et al.*, 2009) erupted just after the flare started (Asai *et al.*, 2008). Imada *et al.* (2007) studied the upflows at the boundary of the dimming in the plage region to the East of the AR, finding an increasing velocity of the upflows with increasing temperature, up to 150 km s^{-1} at $\log T = 6.3$.

Asai *et al.* (2008) used *Hinode*/EIS data from 13 December to make the first spectroscopic observation of a fast-mode MHD shock wave. The faint shock wave originated from AR 10930 and the shock front was observed in *Hinode*/XRT data during the very early stages of the eruption (at 02:23 and 02:24 UT). Asai *et al.* (2008) calculated the expected location of the shock front at 02:36 UT, finding it to lie at least 100″ ahead of the diffuse coronal wave front observed in SOHO/EIT data at that time. Additionally, Asai *et al.* (2008) studied a second, strongly blue-shifted feature located at the southwestern edge of the AR, at ≈350″, −125″ (BS1 in their paper) that appeared during the eruption on the 13 December. This strongly blueshifted region showed velocities of ≈280 and 240 km s^{-1} in the He II and Fe XV lines. Asai *et al.* (2008) associate the strong outflow with a plasmoid ejection seen in *Hinode*/XRT data (they rule out upflows due to chromospheric evaporation).

Jin *et al.* (2009) conducted a detailed study that included investigation of the outflows following the eruption on 13 December. They study the spectra of seven EIS lines and find that outflows exist in the dimmings at a range of temperatures from the lower transition region to the corona. They find that the outflows become stronger in the hotter lines for the recovery following the 13 December event (consistent with the work by Imada *et al.*, 2007). In addition, they find that the magnitude of the outflow velocities are found to be correlated positively with the relative changes of the intensity of the dimming regions, as well as the photospheric magnetic-field strength.

2.2. 14 December 2006 Event

This eruption also originated from AR 10930, and occurred at ≈22:00 UT on 14 December. The LASCO CME catalogue recorded a halo CME at 22:30 UT. The X-ray level peaked with a GOES X1.5-class flare at about 22:12 UT (Kubo *et al.*, 2007). Harra *et al.* (2007) studied the coronal dimming to the East of the AR and, using *Hinode*/EIS data, measured for the first time the velocity of the coronal plasma (≈40 km s^{-1}) in the extended dimming region remote (to the East) from the flare core.

McIntosh (2009) used *Hinode*/EIS data to study the non-thermal line widths in the coronal-dimming region that developed to the East of the AR. He found a rapid increase in the coronal non-thermal line widths, followed by a slow decrease. He concluded that the

growth phase was tied to the post-CME evacuation of the dimming region, consistent with sub-resolution Doppler broadening resulting from the enlarged amplitude of Alfvén waves in an increasingly rarefied plasma. McIntosh (2009) conjectures that as the CME cuts its magnetic ties with the Sun, the corona begins to refill, so that the wave amplitudes shrink back to their nominal (pre-event closed magnetic topology) value.

Jin *et al.* (2009) also studied the outflows following the eruption on 14 December. As for the 13 December event, they found that outflows exist in the dimmings at a range of temperatures from the lower transition region to the corona. For this event, they still find that the outflows become stronger in the hotter lines, but the relationship is weaker than for the outflows following the eruption on 13 December. They report that the magnitude of the outflow velocities following this event are also correlated positively with the relative changes of the intensity of the dimming regions, as well as the photospheric magnetic-field strength.

3. Observations and Data Reduction

3.1. SOHO/EIT Data

EUV imaging data from the *Extreme ultra-violet Imaging Telescope* (EIT: Delaboudinière *et al.*, 1995) onboard the *Solar and Heliospheric Observatory* (SOHO: Domingo, Fleck, and Poland, 1995), at 195 Å is studied from 23:49 UT on 12 December through 15:24 UT on 15 December 2006. EIT data before this time range in December 2006 are not available, due to EIT being in bakeout mode since 25 November.

Coronal dimmings are preferentially studied using "base-difference" images (Figure 2), although they can also be detected in calibrated intensity images of the corona (*e.g.* Figures 3, 4 and 5). Base-difference images have a pre-event image subtracted from all subsequent frames. Thus increases in intensity with respect to the pre-event image (see also Chertok and Grechnev, 2005) appear white and relative decreases in intensity appear dark (black). The EIT data is derotated to 02:00 UT on 13 December and to 21:24 UT on 14 December, in order to produce the base-difference images shown in Figure 2. We note that projection effects can be present in the base-difference data especially where time periods exceeding several hours are considered. Therefore it is important when studying difference images to also make frequent reference to the original intensity data (Chertok and Grechnev, 2005; Attrill, 2010).

For both events, the base-difference data (Figure 2) show that global-scale diffuse coronal waves were observed to accompany the CMEs as well as widespread secondary coronal dimmings.

It should be emphasised that base-difference images show *real intensity changes* with respect to the pre-event image. The appearance of dimmings can be created by displacement (not necessarily removal) of a bright coronal structure, revealing the quiet-Sun emission underneath (Rust and Hildner, 1976). In such a case, plasma evacuation would not be a correct interpretation of the dimming signature. On the other hand, a large-scale loop may well erupt and become a constituent of a CME. As acknowledged in Chertok (2006) and Attrill and Wills-Davey (2010), the only way to ascertain whether or not the bright structure has erupted or simply moved is to study the corresponding original intensity data that corresponds to the dimmed environment identified in the base-differenced data. In order to properly understand the source region of a CME, we must first understand the physical meaning of what the observed dimming signatures actually represent.

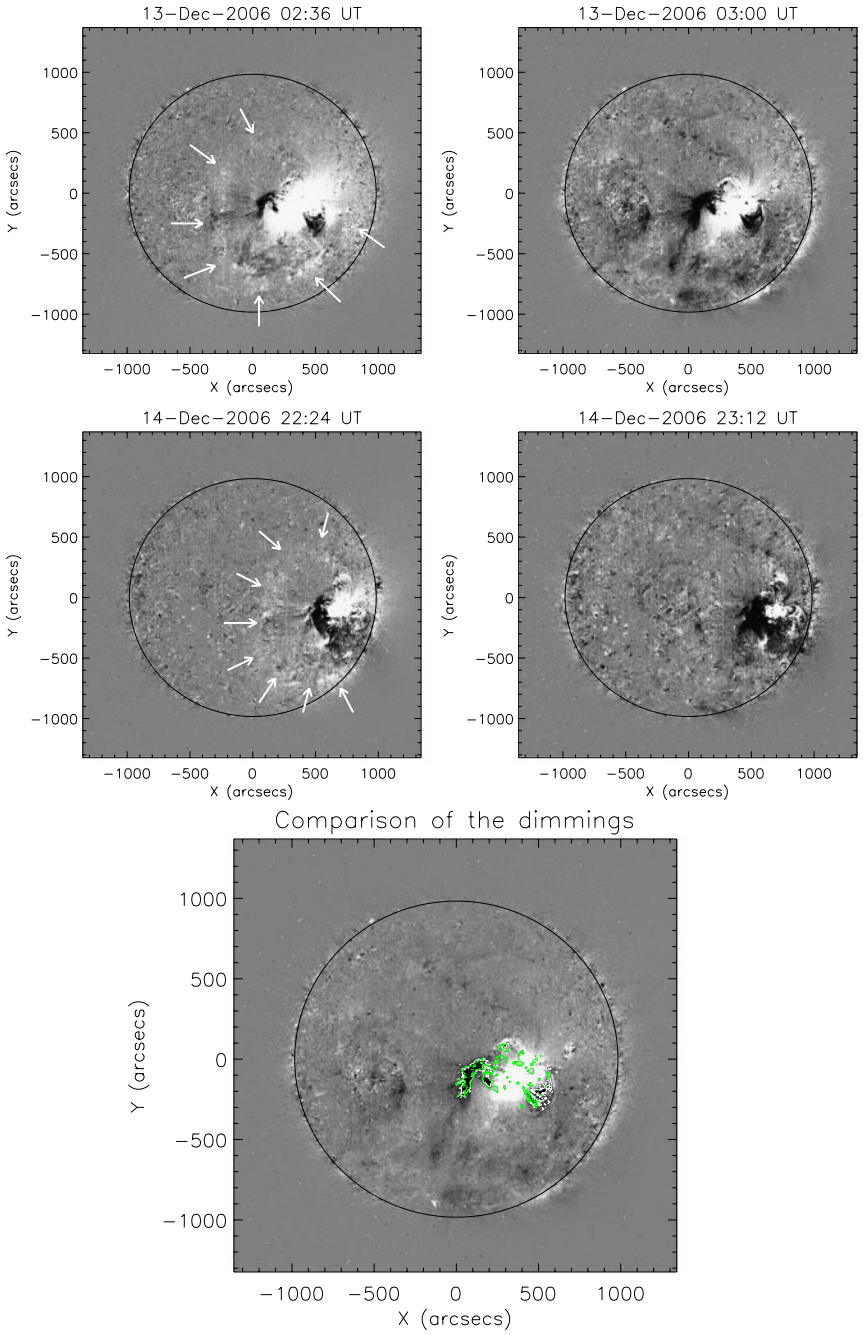

Figure 2 SOHO/EIT 195 Å base-difference images showing the (largely homologous) global coronal waves (white arrows) and dimmings (dark regions) that accompany the eruptions at ≈02:00 UT on 13 December 2006 (top panels), and at ≈22:00 UT on 14 December 2006 (centre panels). Bottom panel shows a direct comparison of the dimmings at 03:00 UT on 13 December (background and white contour), and at 23:12 UT on 14 December (green contour). The data in the bottom panel have been derotated to the same pre-event time at 02:00 UT on 13 December.

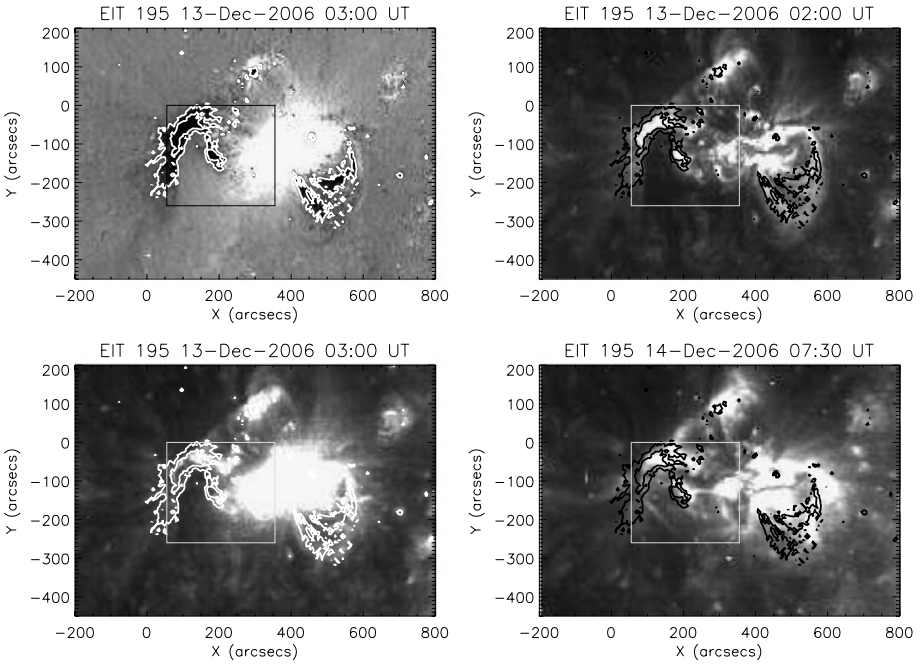

Figure 3 Top left panel shows a SOHO/EIT 195 Å base-difference image following the eruption on 13 December 2006. Contours highlight the coronal dimmings. The original intensity images (other three panels) show EIT data before, during, and after the recovery of the dimmings with the same contours overlaid. The contours correspond to bright regions in the pre-eruption data, showing that the bright plasma is removed during the dimming, but accumulates again as the dimming region recovers, brightening the region within the contours. The dimmings are primarily due to the removal and replenishment of bright coronal loops. The boxes indicate the approximate field of view of the EIS rasters shown in Figure 5.

The main body of the East – West orientated filament that disappeared during the eruption on 13 December appears to be rooted at the location of a strongly blue-shifted feature (BS1 in Asai *et al.*, 2008). The powerful and long-duration flare causes significant saturation and scattered light in the SOHO/EIT images, and we are unable to observe the region at $\approx 350''$, $-125''$ in EIT data. We suggest that the strongly blue-shifted region corresponds to the footpoint of the flux-rope that surrounded the erupting filament. If we had been able to observe this region, we expect that a core dimming would have been found at this location. In view of this, we surmise that the EIT data (Figure 2) show only secondary dimmings, since they are remote from the flare core and so cannot correspond spatially to the erupted filament flux-rope footpoints.

Figures 3 and 4 show base-difference images of the dimmings associated with the two eruptions. Contours have been overlaid highlighting the dimmings observed in each event. Then, these same contours are overlaid on *i*) pre-eruption original intensity EIT data, *ii*) the EIT data during the time at which the dimming was present, and *iii*) EIT data after the eruption, at which time the dimmings have largely recovered. Figures 3 and 4 show that the formation of the dimmings on 13 and 14 December are primarily due to the removal of concentrated knots of bright coronal plasma. The recovery of the dimmings is strongly linked with the formation of new bright loops that connect into the main AR and replace the hot coronal plasma.

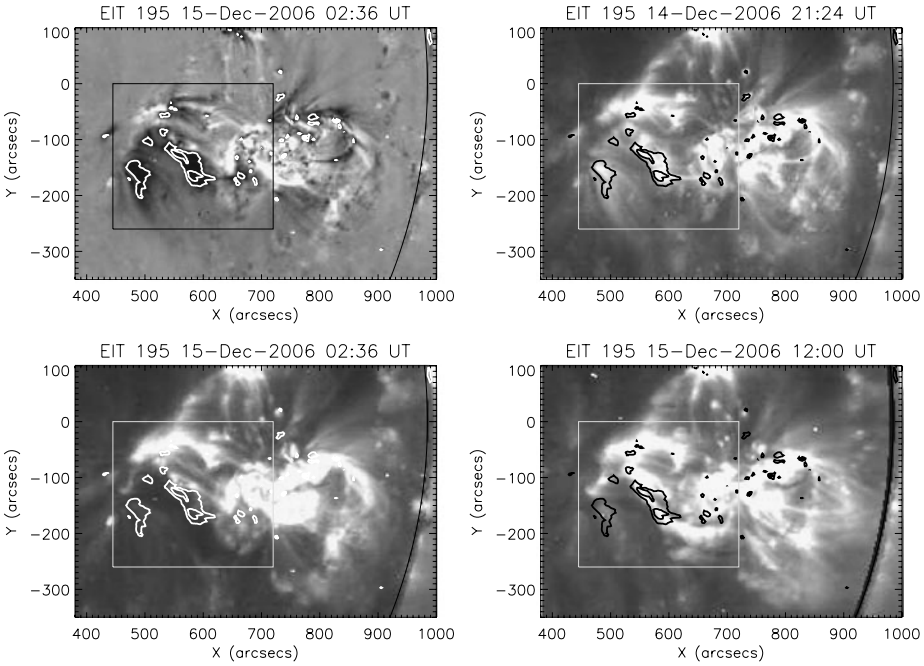

Figure 4 Top left panel shows a SOHO/EIT 195 Å base-difference image following the eruption on 14 December 2006. Contours highlight the coronal dimmings. The other three panels show original intensity images before, during, and after the recovery of the dimmings with the same contours overlaid. The contours correspond to bright regions in the pre-eruption data, showing that the bright plasma is removed during the dimming, but accumulates again as the dimming region recovers, brightening the region within the contours. The boxes indicate the approximate field of view of the EIS rasters shown in Figure 5.

3.2. *Hinode*/EIS Data

We studied the flows in the dimming region to the East of the AR by analysing data from the *EUV Imaging Spectrometer* (EIS: Culhane *et al.*, 2007) onboard the *Hinode* spacecraft (Kosugi *et al.*, 2007). The EIS instrument is a scanning-slit spectrometer observing in two wavebands in the EUV: 170 – 210 Å and 250 – 290 Å. The spectral resolution is equivalent to approximately 34 km s^{-1} pixel^{-1} for the 195 Å emission line, which allows velocity measurements of a few km s^{-1}. The temperature coverage ranges from log $T = 4.7 - 7.3$ with a spatial resolution of close to $1'' - 2''$.

The EIS made a number of rasters that covered the edge of the flaring AR, focusing on the nearby plage region to the East, where coronal dimming occurred. We studied eight EIS rasters made in the Fe XII 195 Å line (see Table 1) starting on 11 December 2006 at 00:25 UT and we analyse the data until the end of the 10:29 UT raster on 15 December 2006 (at 11:12 UT). The rasters all used the $1''$ slit, and the temporal duration of the rasters are several hours because of the large field of view. For each raster we followed the standard calibration procedure using the eis_prep routine in SolarSoft (Freeland and Handy, 1998). The slit tilt and orbital variation of the line position were removed. We concentrated on the strongest emission line (Fe XII) as we are interested in the region of reduced intensity and the relation of the EIS data to observations at 195 Å in the Fe XII line of SOHO/EIT. We fitted each spectrum with a Gaussian profile to determine the Doppler velocity. The rest wavelength was derived from the top right-hand corner of the raster away from the main

Table 1 Details of the eight EIS rasters used in this study. All rasters used the 1″ slit.

Raster	Start time (UT)	Exposure time (s)	# Steps in raster	Raster duration (hr:min)	Study acronym
1	11 December 00:25	30	512	04:16	JTM004
2	12 December 19:07	30	512	04:16	JTM004
3	13 December 01:12	30	512	04:16	JTM004
4	14 December 15:11	10	256	00:43	COMSCI_AR2 _Raster_1
5	14 December 19:20	30	256	02:08	JTM002
6	15 December 01:15	30	256	02:08	JTM002
7	15 December 04:10	30	256	02:08	JTM002
8	15 December 10:29	10	256	00:43	COMSCI_AR2 _Raster_1

activity and strong outflows. Figure 5 shows the intensity and derived velocity maps for each of the eight EIS rasters. We note that EIS rasters from West to East, so that the right side of the rasters are made earlier than the left side. It is important to understand that the EIS data do not represent an image made at a single point in time, rather the rasters presented here range between ≈40 minutes and more than four hours in duration (see Table 1).

3.2.1. Origin of EIS Flows Prior to the 13 December 2006 Eruption

The velocity maps in Figure 5 show velocities in the range ± 40 km s^{-1}, with the exceptions of rasters (aii) and (cii), which show velocities in the ranges ± 30 km s^{-1} and ± 100 km s^{-1}, respectively. The second EIS velocity map (bi), Figure 5 shows strong outflows (blueshifts) in the plage region to the far East (left) of the EIS raster at $\approx(40'', -110'')$, and to the West at $\approx(260'', -100'')$ and $\approx(290'', -60'')$. Comparison of the first EIS intensity raster (ai) on 11 December with the second (bi) on 12 December shows that these outflows develop at the footpoints of coronal loops that existed connecting the AR and plage region. Due to the data gap in EIT data (Section 3.1), we cannot study the dynamics of these changes in the EUV data. However, GOES records multiple B-class and three C-class flares on 11 December associated with AR 10930 (according to the PHTX plots from the CDAW CME catalogue), and six CME eruptions are recorded on 11 and 12 December. Any of these CMEs could be responsible for the reconfiguration of the plage region, dimming, and resulting outflows that we observe in the 12 December raster (bii) in Figure 5. *Hinode*/XRT focuses on the hot plasma of the AR and immediate surroundings, however, XRT synoptic images (not shown) can be used to isolate the dramatic change in coronal configuration to between 13:01 UT and 19:01 UT on 12 December. Further, GOES/SXI does not record any notable flares on 12 December between 13:01 and 19:01 UT, but there is a data gap between 16:30 and 18:54 UT. Examination of GOES-12/SXI imager data does not show any dramatic changes before the data gap at 16:30 UT. We therefore surmise that the eruption causing the dramatic change in coronal connectivity and associated flows (bii) in Figure 5, occurred sometime between 16:30 and 18:54 UT on 12 December. The LASCO CME catalogue records a CME front appearing over the SE limb at 20:28 UT. This is consistent with an eruption from AR 10930 during the GOES data gap. This CME removed the large-scale hot coronal loops (visible in raster (ai)) that connected the AR and plage region, and created the strong outflows observed in (bii).

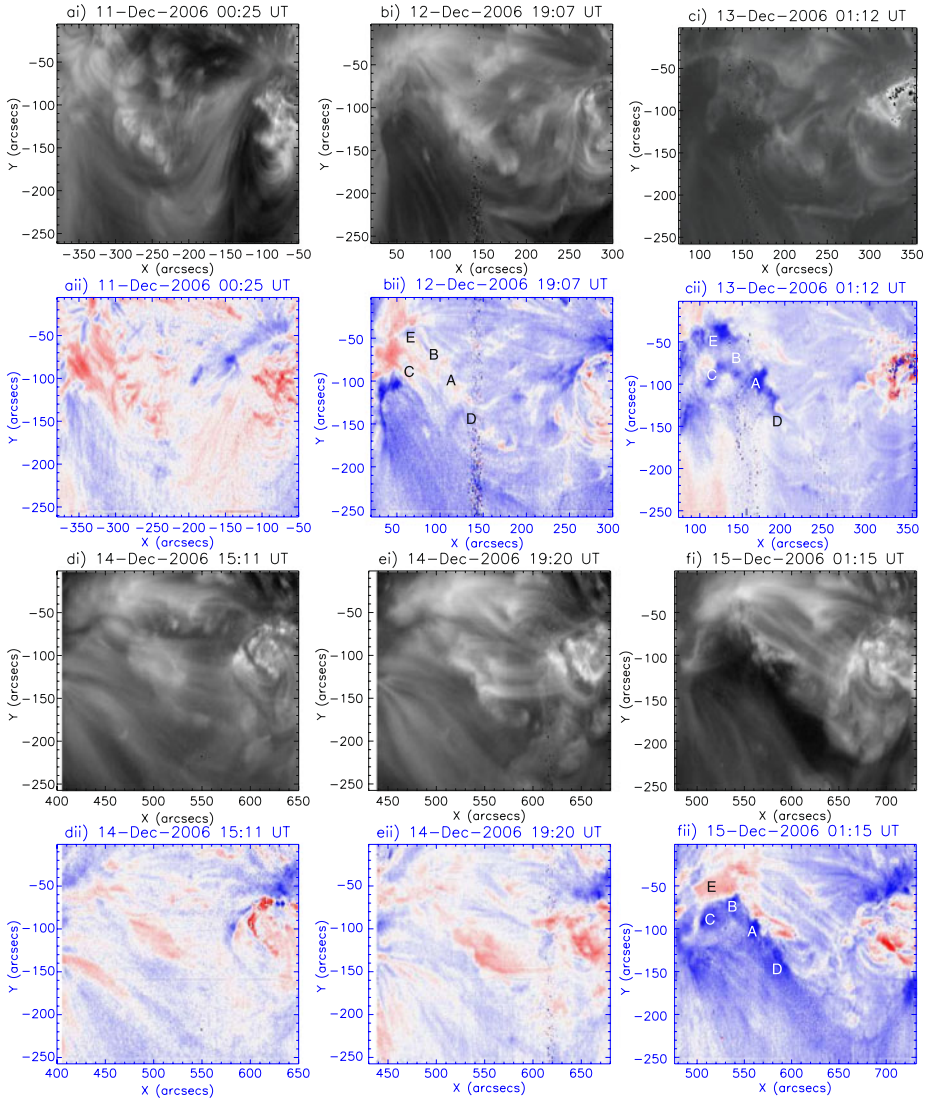

Figure 5 Sequence of eight logarithmically-scaled EIS intensity rasters (greyscale) made in the Fe XII line, and the corresponding velocity maps from 11 December 00:25 UT through 15 December 10:29 UT. The times displayed indicate the start time of each raster. The rasters show approximately the same field of view, as the region rotates from just East of central meridian to near the West limb. The arrows in (hi) indicate bright knots or "pearls" of enhanced emission. The velocity maps are all plotted showing velocities in the range ± 40 km s^{-1}, with the exceptions of rasters (ii) and (cii), which show velocities in the ranges ± 30 km s^{-1} and ± 100 km s^{-1} respectively.

3.2.2. EIS Flows Following the Eruptions

The EIS intensity rasters (Figure 5) show the changing connectivity of the hot coronal loops in the plage region to the East of AR 10930. The formation and recovery of the coronal dimmings can be followed in the sequence of rasters. A striking feature, most noticeable

Figure 5 (*Continued*)

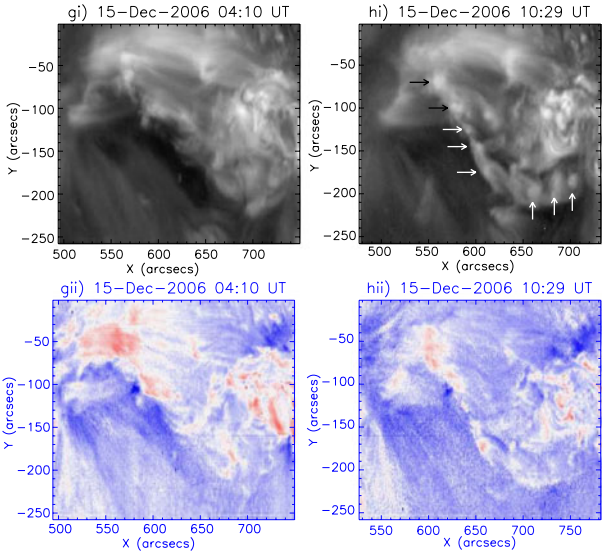

in the last EIS raster (h) which started at 10:29 UT on 15 December, is a chain of bright knots or "pearls" of emission that form at the western edge of the coronal-dimming region, associated with concentrated downflows.

In addition to these concentrated downflows, elongated red shifts are noteworthy features that are seen in some of the EIS rasters. In all cases, these elongated red shifts correspond to relatively long coronal loops that have one end originating in either the AR or plage region. For example, immediately to the Southeast of the AR in the first pre-event raster (a) starting at 00:25 UT on 11 December. These particular downflows do not re-appear in any of the other rasters. In the EIS velocity maps (dii) and (eii), starting at 15:11 and 19:20 UT on 14 December, respectively), following the eruption at ≈02:00 UT on 13 December, elongated red shifts have been established, this time to the far East (left) of the rasters. Following the eruption at ≈22:00 UT on 14 December, these elongated red shifts vanish and do not re-appear in any of the following EIS rasters. In summary, the detailed flows associated with each event are different.

This point is illustrated in Figure 5 by making a direct comparison between the pre-event flows on 11 December (bii) and the flows following the 13 December (cii) and 14 December (fii) events. Some outflows (*e.g.* "A", "C") following the eruption on the 13 December largely disappear and are then re-established following the eruption on the 14 December. The outflows to the North (*e.g.* "E") for the 13 December event are replaced by strong downflows following the 14 December event. Other outflows (*e.g.* "B") intensify, whilst some initially downflowing regions develop strong outflows (*e.g.* "D"). Comparison with the pre-event raster on 12 December (bii) shows that the outflows common to both the 13 and 14 December events (outflows "A", "B", and "C") are originally located in regions associated with downflows (redshifts) in the plage region.

These local differences are due to the coronal magnetic restructuring that occurs amongst the AR and its surroundings between the recovery of the 13 December event and the onset of the 14 December eruption (see EIT 195 Å data shown in Figures 3, 4, and the EIS intensity rasters in Figure 5). It is interesting to make the comparison between the small and large-scale aspects of these events – whilst globally the events appear to be quite homologous

(Figure 2), locally, there are clear differences in the flows associated with the dimming regions in each event.

3.3. Hα Data

Hα data were available for the time period spanning the eruption on 14 December. The Hα data are taken from the PICS instrument at Mauna Loa Solar Observatory, and are shown in Figure 6. In order to coalign the Hα data, it is first mapped to the viewpoint of SOHO (using *SolarSoft's* `map2soho`).

By 17:21 UT on 14 December, a brightening with a ribbon-like morphology developed in the Hα data, remote from the AR (white arrow, top left panel, Figure 6). The brightening disappears by 18:36 UT. It reappears again between 21:39 and 22:09 UT (white arrow, centre left panel, Figure 6), in association with the main flare in the AR. The remote ribbons separate (seen in the Hα movie at 22:15 UT, see `halpha_mlso_141206.mov`), and have disappeared again by 22:27 UT. This remote brightening in Hα data is also observed in EIT 195 Å data (see bottom-left panel, Figure 6). Following the eruption on 14 December, the western boundary of the coronal-dimming region formed at the same location previously occupied by the bright Hα ribbon (Figure 6, bottom-right panel).

Another feature of interest in the Hα data is the apparent formation of a remote plage filament (black arrows, top right panel, Figure 6), by 17:33 UT on 14 December. We emphasise that we do not observe the filament to be co-spatial with the Hα remote ribbon-like brightening. The brightening occurs to the East of the filament. There is no sign of this filament in the Hα data at 02:12 UT, prior to the eruption on 13 December. The southernmost part of the filament disappears during the eruption, but the northern part of the filament survives the eruption on the 14 December and becomes fully developed again by 00:36 UT on 15 December (Figure 6, centre right panel). Figure 7 (top panel) shows the Hα image at 18:36 UT on 14 December, prior to the second eruption. The remote filament is traced with a black dashed line and black arrows. Overlaid are contours of SOHO/MDI data at 19:15 UT at ±50 G (red indicates positive polarity, and blue negative-polarity magnetic field). The remote filament lies along a neutral line in the plage region to the East of the AR.

The relationship of the remote ribbon-like brightening to the magnetic field is shown in the centre panel of Figure 7. The brightening is highlighted by white arrows, and is related to concentrations of positive-polarity magnetic field. During the recovery phase following the eruption, the concentrated bright pearls that form (Section 3.2.2) appear to be associated with the same positive-polarity magnetic elements that were previously associated with the pre-event brightening (bottom panel, Figure 7).

3.4. *Hinode*/XRT Data

Full-disk synoptic images (Figure 8) from the *Hinode*/X-ray telescope (XRT: Golub *et al.*, 2007), show a change of the global-scale hot coronal loops observed between 00:51 UT and 07:01 UT – spanning the timeframe of the 13 December eruption ≈02:00 UT. The new, hot XRT loops in the northern hemisphere (white arrow, seen five hours after the eruption) form at the same location as the remote weak EUV dimmings (see Figure 2). These data link the remote dimmings to the global magnetic restructuring that was likely associated with this CME and further support the idea that remote coronal dimmings are likely to be due to plasma evacuation during a CME (see Section 1.3). The new loops had disappeared

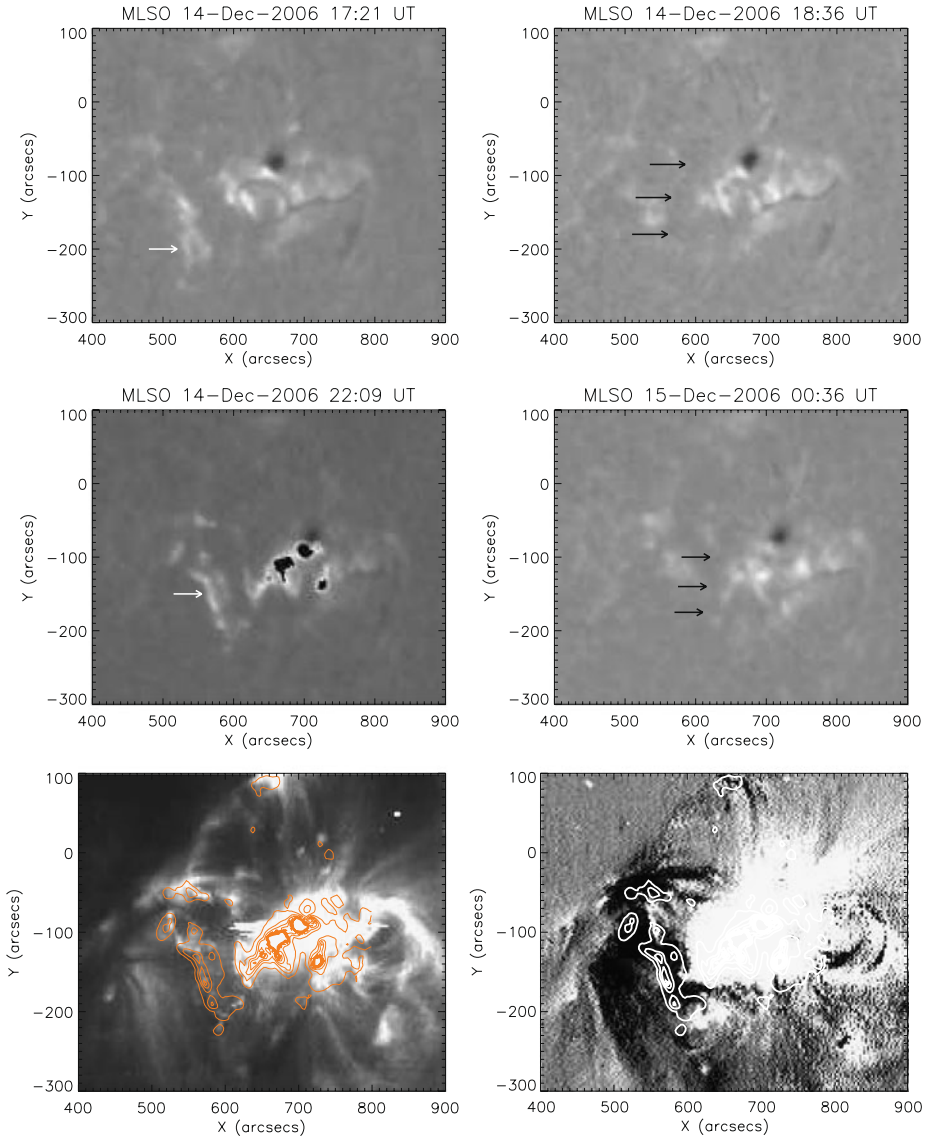

Figure 6 Top panels: MLSO Hα data showing the activity near the location of the eastern dimming region, from 17:21 UT on 14 December until 00:36 UT on 15 December. (The Hα data at 22:09 UT show black patches, which indicate saturation of those pixels). White arrows indicate a ribbon-like remote brightening, to the East of the AR. Black arrows point to a filament, also remote and to the East of the active region. The bottom-left panel shows EIT 195 Å data at 22:12 UT on 14 December, overlaid with Hα contours (orange) at 22:09 UT highlighting the remote bright ribbon-like feature to the East of the AR. The bottom-right panel shows EIT base-difference data, with the coronal dimming (black) at 22:24 UT. Overlaid are the co-aligned Hα data at 22:09 UT (white) showing the location of the bright ribbon-like feature, prior to the eruption. The reader is encouraged to view the Hα movie: `halpha_mlso_141206.mov`.

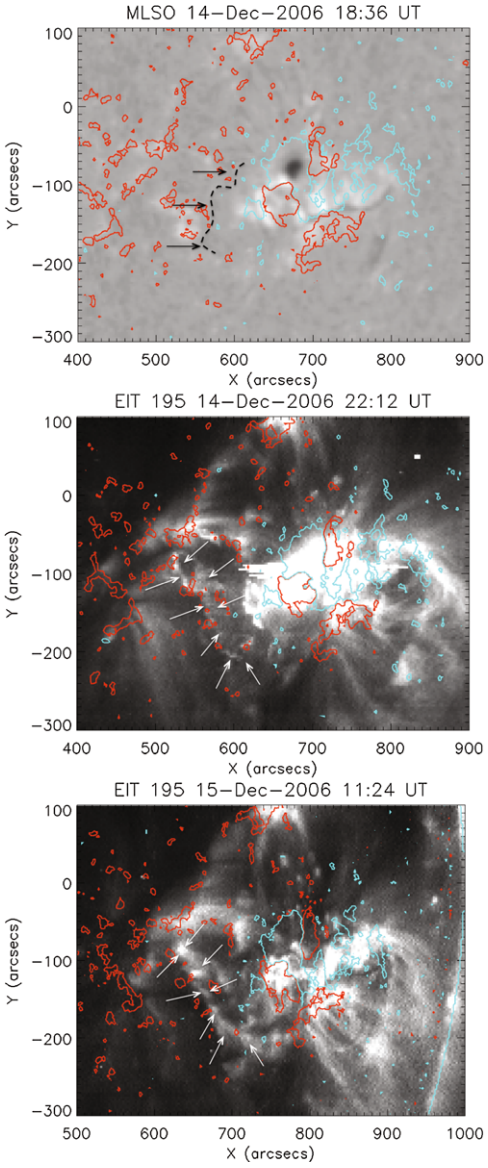

Figure 7 Top panel shows the Hα image at 18:36 UT on 14 December. The remote filament is traced with a black dashed line and black arrows. Overlaid are contours of SOHO/MDI data at 19:15 UT at ±50 G (red indicates positive polarity, and blue negative polarity magnetic field). Centre panel: EIT 195 Å image at 22:12 UT showing the remote brightening that develops just prior to the eruption on 14 December, with MDI contours at 22:27 UT overlaid. Bottom panel shows the post-eruption EIT 195 Å image "pearls", with MDI contours at 11:11 UT overlaid.

in the XRT data by the time of the next synoptic at 07:01 UT on 14 December. No new bright loops were seen in XRT data following the eruption at ≈22:00 UT on 14 December, although the next synoptic was not available until 07:12 UT on 15 December, nine hours after the eruption. It is therefore possible that new loops formed and then cooled during this time.

Figure 8 also highlights dramatic changes that occurred during this event, specifically noticeable in the altered hot coronal loops located to the East of the AR. The most obvious change (removal of hot coronal material) occurs at the location of coronal dimming observed in the EIT data (see bottom panel, Figure 2).

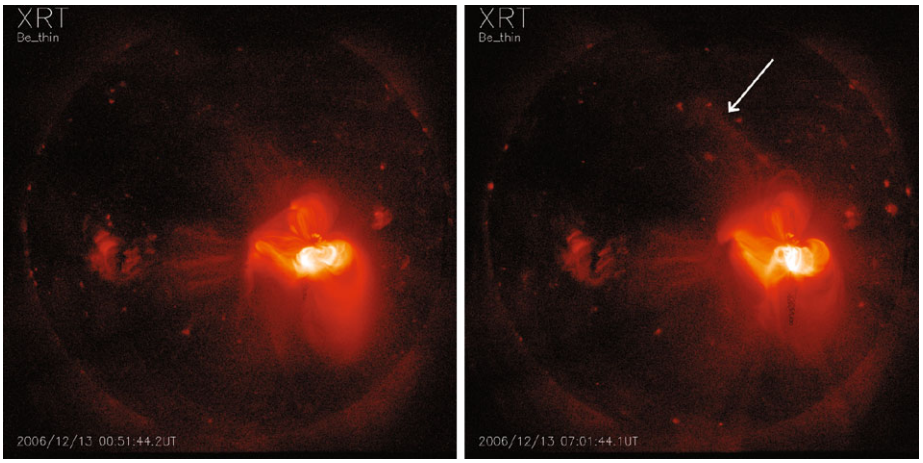

Figure 8 *Hinode*/XRT synoptic images taken using the thin Be filter on 13 December 2006 at 00:51 and 07:01 UT (left and right panels, respectively). The images show evidence for the formation of new hot loops (white arrow). It is likely that these large-scale changes are associated with global magnetic restructuring that occurred, following the CME at ≈02:00 UT. It is noteworthy that these new hot loops form at the same location as remote weak dimmings seen in EUV data (see Figure 2). Changes in the plage region to the East of the AR are also evident. The disappearance of hot plasma occurs at the same location as coronal dimming observed in EUV data (bottom panel, Figure 2).

4. Results

4.1. Outflows

Early in the recovery phase following the 14 December event, overlays of the EIS velocity map with SOHO/MDI data reveal a correspondence of the strongest EIS outflows (≈ -50 km s^{-1}) with the positive-polarity magnetic concentrations (Figure 9, centre panel). Doschek *et al.* (2008) also reported a correspondence between the locations of outflows in ARs measured by EIS and the underlying morphology of the longitudinal photospheric magnetic flux. Jin *et al.* (2009) examine the detailed relationship between the magnetic-field strength and the outflow velocity for the 13 and 14 December 2006 events and find in both cases that the outflows are concentrated at patches with a strong photospheric magnetic field. The larger the magnetic-field strength, the faster the outflow velocity. Jin *et al.* (2009) derive correlation coefficients of ≈0.65 and ≈0.58 for the two events, respectively. Although statistically significant, these correlations are not one-to-one, and there are clearly strong positive magnetic concentrations that are not associated with significant outflows (*e.g.* centre panel, Figure 9). Although the Fe XII emission (and associated flows) could originate from the movement of plasma in large-scale overlying coronal loops (so explaining the lack of correlation with photospheric magnetic elements), here we suggest that the outflows do correspond to loop footpoints. We favour this interpretation due to the location of the strongest outflows being concentrated at the footpoints of coronal loops seen in the EUV data (Figures 3, 4, and 5). Similar results were found by Harra *et al.* (2008) for outflows at the periphery of an AR studied during February 2007. Additionally, the onset of the strongest outflows occurs in association with the two CME events, so that the formation of the outflows at the loop footpoints is consistent with those loops being reconfigured and expanded to form the

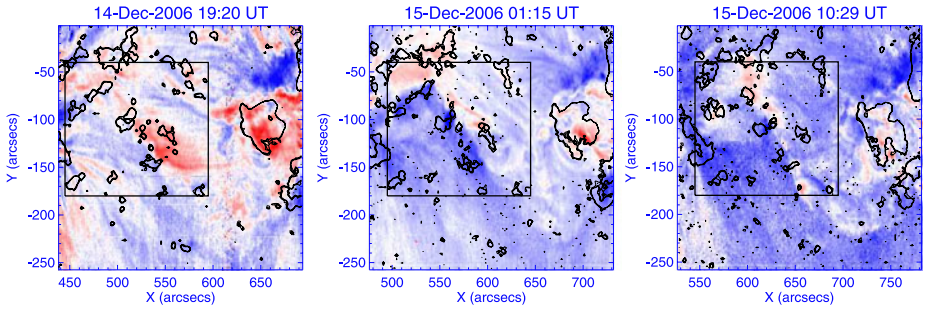

Figure 9 EIS velocity maps overlaid with MDI contours of positive-polarity magnetic concentrations (black). In the centre panel (raster following the 14 December eruption), the concentrated outflows are associated with the magnetic concentrations. In the later raster (right panel), following the recovery of the dimmings, the positive-polarity elements are associated with red shifts indicating downflowing plasma.

CME. Overlying loops would be removed by the expanding CME so although we believe that they are important for understanding the flows before the CME and during the recovery phase of the dimmings, as the CME departs the Sun the newly opened magnetic-field lines dominate. Given this interpretation, we suggest that the lack of a one-to-one correlation of outflow concentrations with photospheric magnetic-field elements results because not all elements are associated with coronal loops. There are many positive magnetic elements that exist within the low-latitude coronal hole that do not correspond to the footpoints of large-scale coronal loops. Only coronal loops that are involved in the eruption are physically able to drive significant outflows in the form of plasma evacuation, concentrated at the footpoints of the greatly expanded ("opened") loops.

4.2. Downflows

Figure 5 shows that in the eighth raster (hii), starting at 10:29 UT on 15 December, the knots of red shifted plasma have moved Southeast (compared to the pre-event – second (bii) – raster on 12 December, and the sixth raster (fii) starting at 01:15 UT on 15 December). Approximately 15 hours into the recovery phase following the eruption on 14 December, overlays of the EIS velocity map with SOHO/MDI data reveal that downflows have developed at the locations previously dominated by significant outflows. These downflows are found to overlie MDI positive concentrations (right panel, Figure 9).

4.3. Recovery of EIT Intensity and Reduction of EIS Outflow Velocity

Figures 10 and 11 show lightcurves of the average intensity within three concentrated outflow regions (red, orange, and green) for each event as a function of time. The onset of the coronal dimming in each concentrated outflow region is marked by a dramatic drop in the corresponding EUV intensity level. In both events, the recovery is characterised by a gradual recovery process, typical of coronal dimmings (see *e.g.* Reinard and Biesecker, 2008; Attrill *et al.*, 2008).

The outflow velocity of three concentrated regions following the 14 December event (red, orange, and green) was also measured by EIS as a function of time over multiple rasters (Figure 12). It should be noted that the outflow disappeared and started again after the eruption on 14 December (see Figure 5), but in the plots shown in Figure 12, we focus only on the outflow velocities, the downflow velocities are not shown. Following the 14 December

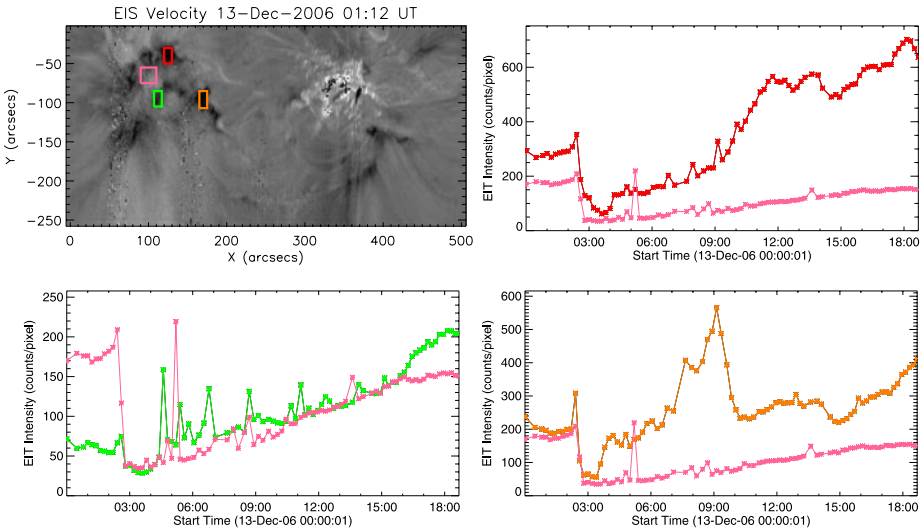

Figure 10 Following the 13 December eruption: EIS Fe XII velocity map showing three concentrated outflows (red, orange, and green regions) and a region of weak outflow in a region of reduced intensity (pink box, see Figure 13). Lightcurves show the corresponding intensity evolution of EIT Fe XII emission in the different regions.

eruption at ≈22:00 UT, the last three points of the EIS outflow plots shows that the outflow velocity slows increasingly gradually. By the time of the 15 December raster that starts at 10:29 UT, evidence of the outflows have almost disappeared.

Comparing the EIS outflow velocities and EIT lightcurves of Figure 11, we can see that as the outflow velocity reduces, the intensity also recovers. By 11:00 UT on 15 December, although the intensity has not completely recovered to pre-event values by this time, it has recovered significantly.

5. Discussion

5.1. Common Aspects of Both Events

The secondary dimmings associated with the eruptions on the 13 and 14 December are formed at the locations of bright coronal loops, in the plage region remote to the East of the main AR. The dimmings are due mainly to the removal of concentrated knots of hot coronal plasma. The recovery shows that these bright knots are associated with overlying coronal loops that connect into the heart of the AR.

Both of the events produce global-scale, diffuse coronal waves and halo CMEs. Both were associated with X-class flares, which occurred at similar locations within the AR. The dimmings for each event occur in the same extended area (Figure 2), and are associated with the bright coronal loops to the East of the AR (see Figures 3 and 4). In both events, outlying, less bright coronal loops are also removed. Chertok (2006) reports a series of nine global and homologous events in November 2004 that showed recurrent systems of large-scale dimmings, similar to the events studied here.

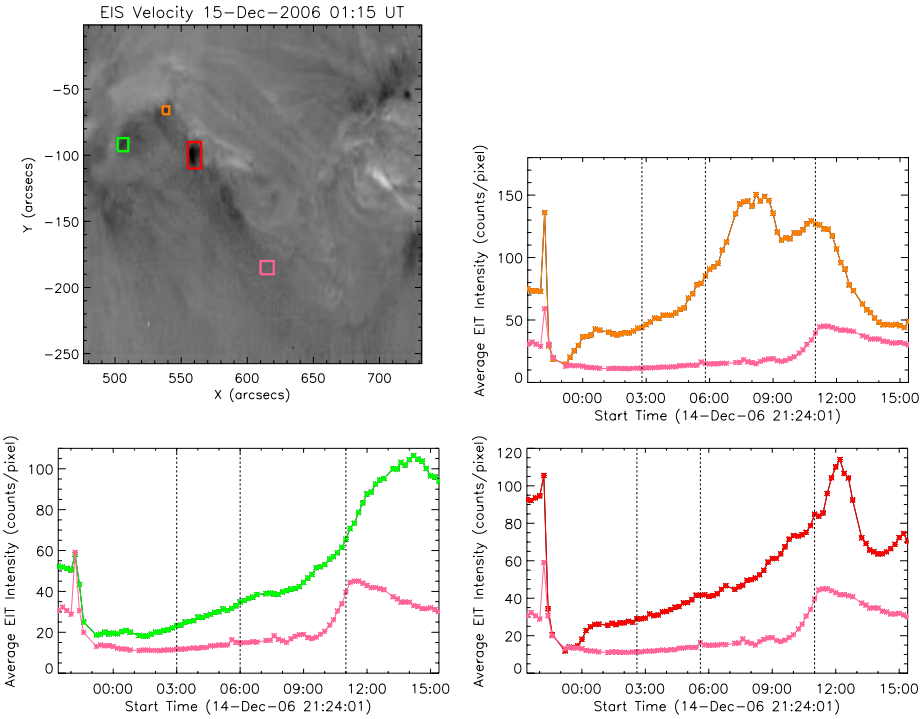

Figure 11 EIS Fe XII velocity map showing three concentrated outflows (red, orange, and green regions), and a region of weak outflow in a region of reduced intensity (pink box, see Figure 13). Lightcurves show the corresponding intensity evolution of EIT Fe XII emission in the different regions. The dashed vertical lines correspond to the times at which the EIS slit passes the location of the strong outflow regions in the EIS rasters (shown in Figure 12).

5.2. Formation of the Dimmings and Initial Recovery Phase

The dimmings can be seen in the non-differenced EIT and EIS intensity data (Figures 3, 4, and 5). This is usually interpreted as a signature that the low corona has "opened" during the eruption (as in the famous 12 May 1997 case with the transient coronal holes, observed by SOHO/EIT and *Yohkoh*/SXT), where the mean intensity can drop below that of the surrounding quiet-Sun environment, toward the intensity of pre-existing coronal holes (see, *e.g.*, Rust, 1983; McIntosh *et al.*, 2007; Attrill *et al.*, 2006, 2008). However, we noted in Figure 1 that for the 13 and 14 December 2006 events, the whole AR complex and surroundings are located in the midst of a reduced-intensity region, that was originally a low-latitude coronal hole. Therefore care should be taken with interpretation of this event since a drop to coronal-hole intensity level could be produced along the line of sight simply by a removal of overlying coronal loops.

Figure 13 shows scatter plots of EIS velocity measurements as a function of intensity. The plots are made from the rasters starting at 01:12 UT on 13 December, with the slit reaching the location of the strong outflows around 04:30 UT, and at 01:15 UT on 15 December, with the slit reaching the location of the strong outflows around 02:36 UT. As such, the measurements shown in the scatter plots are made at snapshots in time as the EIS slit moves across the location of each box. These results show that the strongest outflow regions (red, orange, and green boxes) for each event at these times during the recovery phase

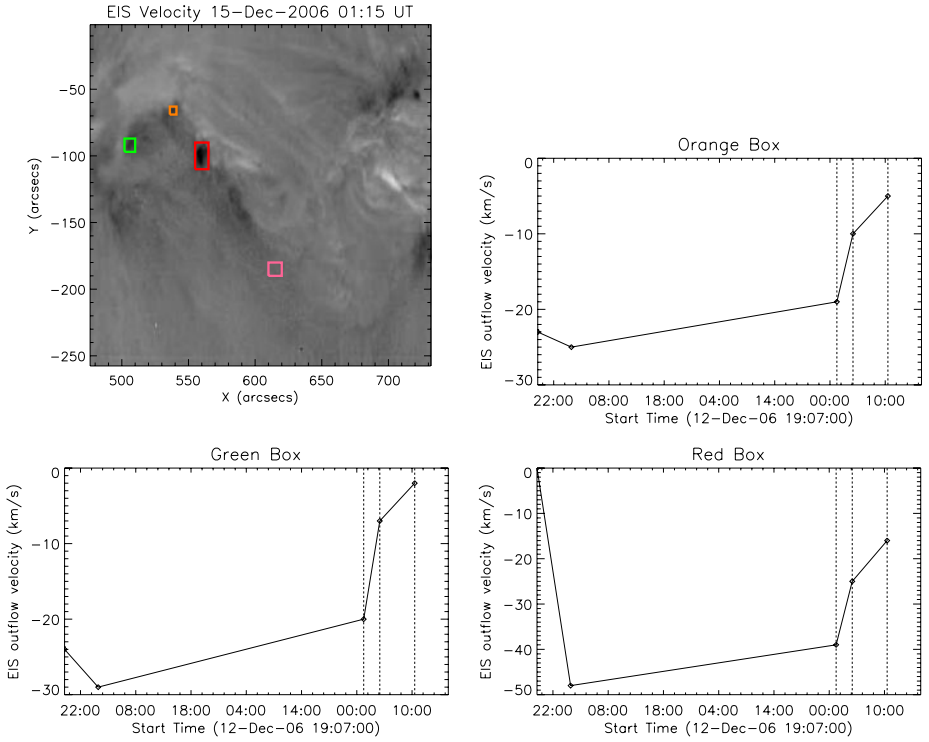

Figure 12 EIS Fe XII velocity map showing three concentrated outflows (red, orange and green regions) and a region of weak outflow in a region of reduced intensity (pink box, see Figure 13). Plots show the evolution of the EIS outflow velocities for each concentrated outflow region (red, orange, and green). EIS downflow velocities are not shown in these plots. The measurements are made when the EIS slit passes the location of the strong outflow regions in the EIS rasters. The measurements highlighted by dashed vertical lines correspond to EIT intensity as shown in Figure 11.

correspond to regions of relatively high intensity compared to the region of low intensity (pink boxes). Specifically, for the 13 December event, the red, orange, and green regions have mean intensities of 624, 701, and 209 counts pixel^{-1}, corresponding to mean outflow velocities of -57, -58, and -28 km s^{-1}, respectively. The low intensity (pink) region has a mean intensity of 105 counts pixel^{-1}, but an outflow velocity of just -9 km s^{-1}. In a similar way, for the 14 December event, the red, orange, and green regions have mean intensities of 380, 669 and 516 counts pixel^{-1}, corresponding to mean outflow velocities of -30, -22 and -21 km s^{-1}, respectively. The low intensity (pink) region has a mean intensity of 125 counts pixel^{-1}, with an outflow velocity of just -11 km s^{-1}. Thus in both events, the strongest outflow regions correspond to relatively strong emission as detected by EIS.

In order to understand the intensity evolution of the strong outflow regions, EIT data with a higher temporal cadence are used to place the EIS results in context. We refer again to Figures 10 and 11 which show the mean intensity of the strong outflow regions as a function of time. The pink lightcurve for each event corresponds to a region of low intensity, but minimal flow (see top and centre panels Figure 13). As discussed above, due to the formation of the AR in what was originally a low-latitude coronal hole (Figure 1), the pink lightcurve is indicative of coronal-hole intensity level, which is understood to correspond

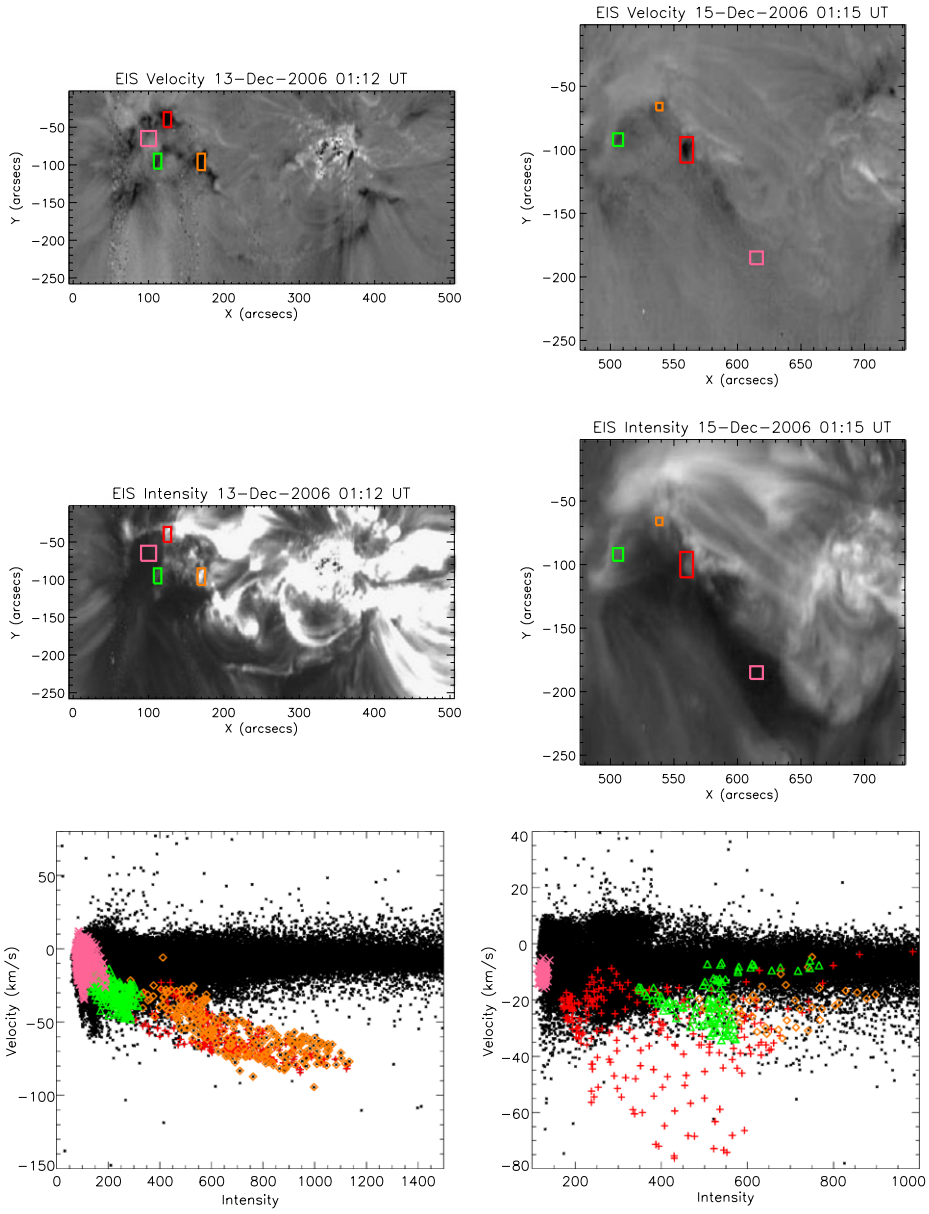

Figure 13 Top (centre) panels show EIS velocity (intensity) maps for the rasters commencing at 01:12 UT on 13 December and 01:15 UT on 15 December (left and right panels, respectively). Coloured boxes: red, orange, and green, are located where EIS measures a significant blueshift in each raster. The pink boxes are located at regions of weak emission. The bottom panels show scatter plots of EIS intensity versus outflow velocity. Black points show data for the entire raster, coloured points correspond to data from the coloured boxes. In both cases, the lowest intensity is found in the pink box, but this region only shows a relatively weak outflow compared to the other coloured regions.

to a region of dominantly "open" magnetic-field lines. For both events, the red, orange, and green lightcurves in Figures 10 and 11 all drop to approximately the pink coronal-hole intensity level within the first 30 minutes following the onset of the dimming. Within two hours, each outflow region shows a significant recovery in intensity. This behaviour is typical of the onset and recovery phase of coronal dimmings (*e.g.* Chertok and Grechnev, 2005; Attrill *et al.*, 2006, 2008; Reinard and Biesecker, 2008).

5.3. Structure of the Dimmings and Associated Flows

Previous work examining the intensity variation within coronal dimmings in EUV data has shown that the interior has a non-uniform distribution (*e.g.* Attrill *et al.*, 2008). Figures 3 and 4 confirm this result for the 13 and 14 December dimmings as well. In these December 2006 events, we only observe significant EIS outflows in concentrated patches within the wider dimming that are picked out in the base-difference data. The EIS velocity maps in Fe XII are really dominated by structured loop-like flows. Why do we not observe significant outflows from all over the dimmed region? Because the wider dimmings are actually the result of the removal of coronal loops, whose footpoints end only in the concentrated dimming patches (Figure 5). Interestingly, although the strongest outflows (red, orange, and green regions; Figures 10 and 11) all show drops in intensity to near the coronal-hole (pink region) level, the strongest outflows persist, even when the intensity has started to recover (Figure 13).

Due to *i*) the presence of the low-latitude coronal hole (Figure 1), *ii*) evidence for the removal of overlying coronal loops (Figures 3, 4 – 5), *iii*) lack of a significant recovery in intensity (pink lightcurves, Figures 10 and 11), and *iv*) only a relatively weak outflow (pink regions, Figure 13), we conclude that the extended dimmings do not show a true "opening" and evacuation of quiet-Sun plasma, rather the extended dimming can be primarily attributed to the removal of overlying coronal material exposing the coronal hole underneath. During the formation of the dimmings, the coronal plasma is only truly evacuated at the footpoints of the coronal loops that become "opened" in these events (red, orange, and green regions; Figures 10 – 13).

5.4. Recovery of the Dimmings

Jin *et al.* (2009) propose that the dimming-region recovery for these December 2006 events is mainly due to the dynamic response of the transition region (TR) to the enhanced pressure gradient as the CME eruption evacuates the plasma in the low corona. They consider that there is a significant mass supply from the lower TR to refill the coronal dimmings, so in this case the upflowing TR plasma is understood to contribute to the recovery of the dimmings.

The analysis we have presented shows that the main reason for the recovery in the intensity is due to the reformation of overlying large-scale bright coronal loops (*e.g.* see Figures 3 and 4). Whilst there may be some mass supply from the lower TR, in these 13 and 14 December 2006 events, the main recovery in the dimmed regions is due to the (re-)establishment of overlying coronal loops. This scenario explains the red – blue – red shifts that are observed (Figures 5, panels (bii), (cii), and (fii) in that the loops are initially closed – loops "opened" – loops closed again. In particular, the development of red shifts in regions previously occupied by outflowing plasma may be interpreted as evidence that these outflow regions are recovered by the formation of overlying coronal loops. In this picture, the re-establishment of the red shift flows is a result of the changing magnetic connectivity. If the recovery is primarily due to outflows from the TR refilling the corona as Jin *et al.* suggest, then we would

expect that the TR outflow would just decrease as the corona is refilled and the pressure gradient is reduced. Thus the blue shift should just reduce to stabilise around a zero shift. It is not clear in their scenario why significant downflows would be re-established. From the EIT and EIS intensity maps (Figures 3, 4, and 5), it seems instead that the large-scale coronal loops re-form (albeit in a slightly altered magnetic configuration).

Since secondary dimmings may be formed by the "opening" of the magnetic-field as a result of the CME expansion through reconnection with the ambient magnetic field (see Section 1.3), these dimmings could recover by reconnection along the long current sheet which formed under the departed CME. This process is the same as the formation of AR flare loops and flare ribbons, but in the case of secondary dimmings the footpoints are more scattered. The new coronal loops formed in place of the dimmings may therefore indicate heating by re-closing reconnection, and they would then connect the former dimming (outflow) footpoints to the region from which the eruption was initiated. This process helps to create an anemone-like structure of, and around, the AR, just as we observe (see Figures 3, 4, 5, and 8).

5.5. Implications for Estimates of CME Mass from Coronal Dimmings

Despite significant uncertainties associated with estimating CME masses, efforts are sometimes made to relate the plasma removed from the coronal-dimming region to the mass of the associated CME (see, *e.g.*, Sterling and Hudson, 1997; Harrison and Lyons, 2000; Wang *et al.*, 2002; Zhukov and Auchère, 2004; Jin *et al.*, 2009). Typically only dimming regions close to the associated flare are considered, and then a bulk plasma density is assigned to the entire dimming region. This study highlights the detailed structure and cause of coronal dimmings observed in EUV data. In the future, more refined estimates should strive to identify which regions truly "open" to evacuate the corona fully, and which dimmings may be caused by a removal of overlying (more rarefied) plasma. Additionally, the role of relatively weak and remote global-scale coronal dimmings (see, *e.g.*, Figure 2) should be evaluated, with a growing body of evidence suggesting that like core coronal dimmings, these are also due to plasma evacuation (see, *e.g.*, Harra *et al.*, 2007; Attrill *et al.*, 2007; Cohen *et al.*, 2009). Studies of the physical cause of coronal dimmings and association to related CMEs have implications for developing our understanding of the genesis and detailed structure of CMEs. Widespread dimmings suggest that the CME constituents may be drawn from a much wider area than is traditionally considered.

5.6. Relationship of Coronal Dimming Outflows to the Solar Wind

It has been suggested by Sakao *et al.* (2007), Harra *et al.* (2008), and Baker *et al.* (2009) that continuous outflows (on timescales of days) at the periphery of ARs are candidates for contribution to at least part of the slow solar wind. These previously reported outflows have relative velocities as measured by EIS of $\approx$50 km s^{-1} so appear to have similar magnitudes and lifetimes as the flows reported here (Sections 5.2 and 4.3, respectively). Additionally, there is evidence from both interplanetary scintillation results and *in-situ* data that the slow solar-wind source is located at the boundary between coronal holes and ARs (*e.g.* Kojima *et al.*, 1999, Ko *et al.*, 2006). In the events that we study here, we have noted that the AR is embedded in a low-latitude coronal hole (Figure 1), so that the dimmings indeed form at just such an interface. However, the major difference is that our flows occur as a direct consequence of the significant expansion of the magnetic field during a CME, whereas the flows at the periphery of ARs exist independent of a CME.

It remains an open question whether the outflows from CME-related coronal-dimming regions contribute (temporarily) to the highly variable speed of the slow, or fast, solar wind. The literature appears to favour a connection with the latter. Coronal dimmings are also known as transient coronal holes (TCHs: Rust, 1983), and it is well-recognised that the fast solar wind emanates from coronal holes (Noci, 1973). Studies have been motivated by the idea that high-speed solar wind flows following CMEs could come from TCHs (*e.g.* Kahler and Hudson, 2001), indeed case-study events such as the well-known 12 May 1997, TCH event was identified (from a numerical coronal outflow model) as the source of a moderately fast solar-wind stream that interacted with the CME (Odstrcil, Pizzo, and Arge, 2005). Due to the similarity of the physical properties of the plasma and magnetic-field structure in both TCHs and long-lived coronal holes, McIntosh *et al.* (2007) and McIntosh (2009) argue that the term TCH is more than a "throwaway" designation, and that the association of fast solar-wind streams with coronal dimmings is real. Detailed spectroscopic measurement and statistics on the outflows from coronal-dimming regions are essential in order to properly determine their contribution to the solar wind.

6. Conclusions

The dimmings in the *Hinode*/EIS field of view for the 13 and 14 December 2006 events are *i*) remote from the AR and flare, *ii*) clearly linked to the removal of bright coronal plasma, and *iii*) recover due to the reformation of bright coronal plasma knots related to coronal loops linked to the main AR (the exact configuration changes between the eruptions, reflected by the complexity of the flows). Therefore for both of these events, we observe secondary dimmings only.

Within the secondary dimmings there are concentrated patches of strong outflow ($\approx$ tens of km s^{-1}) that correspond to a significant intensity depletion, similar to pre-existing coronal-hole levels. These concentrated outflows are located at the footpoints of large-scale coronal loops and in this way are also associated with corresponding magnetic-field elements. The significant outflows are maintained during the recovery phase of the coronal dimmings, although they gradually reduce and are replaced by downflows, as the intensity of the dimmings recovers.

Despite the global homology of the two eruptions on 13 and 14 December 2006, *Hinode*/EIS reveals that on a local scale there are substantial differences, particularly in the flows (and therefore the precise source regions of the CME plasma) associated with the "opened" field in these events.

This work highlights the importance of a case-study approach when studying coronal dimmings. A reduction in coronal intensity indicating coronal dimmings can be detected automatically (*e.g.* Podladchikova and Berghmans, 2005; Reinard and Biesecker, 2008; Attrill and Wills-Davey, 2010), but the interpretation of a measured intensity decrease must be quantified and carefully considered. As this study has demonstrated, a multi-wavelength approach is required as well as placing the event in context with global observations.

Acknowledgements We sincerely thank the referee for their comments and particularly for encouragement in developing the discussion. We thank Yingna Su for helpful discussion regarding the flare ribbons that developed in these events, and we acknowledge the hard work of the *Hinode*/EIS and SOHO/EIT teams for providing the data used in this study. *Hinode* is a Japanese mission developed and launched by ISAS/JAXA, with NAOJ as domestic partner and NASA and STFC (UK) as international partners. It is operated by these agencies in co-operation with ESA and NSC (Norway). SOHO is a project of international co-operation between ESA and NASA. We acknowledge the PICS instrument at Mauna Loa for providing the Hα data. The

EIS Observing Timeline (http://solar-b.nrl.navy.mil/cgi-bin/timeline4.cgi), and the *Hinode*/EIS website hosted at MSSL (http://msslxr.mssl.ucl.ac.uk:8080/SolarB/) were used extensively in this work. GDRA and MWD gratefully acknowledge NASA grant NNX08BA97G. LvDG acknowledges funding through the Hungarian Science Foundation grant OTKA K81421 and the European Community's FP7/2007 – 2013 programme through the SOTERIA Network (EU FP7 Space Science Project No. 218816).

References

Asai, A., Hara, H., Watanabe, T., Imada, S., Sakao, T., Narukage, N., Culhane, J.L., Doschek, G.A.: 2008, Strongly blueshifted phenomena observed with *Hinode* EIS in the 2006 December 13 Solar flare. *Astrophys. J.* **685**, 622 – 628. doi:10.1086/590419.

Attrill, G.D.R.: 2008, Low coronal signatures of coronal mass ejections. PhD thesis, University College London.

Attrill, G.D.R.: 2010, Dispelling illusions of reflection: a new interpretation of the 19 May 2007 event. *Astrophys. J.*, submitted.

Attrill, G.D.R., Wills-Davey, M.J.: 2010, Automatic detection and extraction of coronal dimmings from SDO/AIA data. *Solar Phys.* **262**, 461 – 480. doi:10.1007/s11207-009-9444-4.

Attrill, G., Nakwacki, M.S., Harra, L.K., van Driel-Gesztelyi, L., Mandrini, C.H., Dasso, S., Wang, J.: 2006, Using the evolution of coronal dimming regions to probe the global magnetic field topology. *Solar Phys.* **238**, 117 – 139. doi:10.1007/s11207-006-0167-5.

Attrill, G.D.R., Harra, L.K., van Driel-Gesztelyi, L., Démoulin, P.: 2007, Coronal "wave": magnetic footprint of a coronal mass ejection? *Astrophys. J. Lett.* **656**, L101 – L104. doi:10.1086/512854.

Attrill, G.D.R., van Driel-Gesztelyi, L., Démoulin, P., Zhukov, A.N., Steed, K., Harra, L.K., Mandrini, C.H., Linker, J.: 2008, The recovery of CME-related dimmings and the ICME's enduring magnetic connection to the Sun. *Solar Phys.* **252**, 349 – 372. doi:10.1007/s11207-008-9255-z.

Attrill, G.D.R., Engell, A.J., Wills-Davey, M.J., Grigis, P., Testa, P.: 2009, *Hinode*/XRT and STEREO observations of a diffuse coronal "wave"-coronal mass ejection-dimming event. *Astrophys. J.* **704**, 1296 – 1308. doi:10.1088/0004-637X/704/2/1296.

Baker, D., van Driel-Gesztelyi, L., Mandrini, C.H., Démoulin, P., Murray, M.J.: 2009, Magnetic reconnection along quasi-separatrix layers as a driver of ubiquitous active region outflows. *Astrophys. J.* **705**, 926 – 935. doi:10.1088/0004-637X/705/1/926.

Berger, T.E., de Pontieu, B., Fletcher, L., Schrijver, C.J., Tarbell, T.D., Title, A.M.: 1999, What is moss? *Solar Phys.* **190**, 409 – 418. doi:10.1023/A:1005286503963.

Bewsher, D., Harrison, R.A., Brown, D.S.: 2008, The relationship between EUV dimming and coronal mass ejections. I. Statistical study and probability model. *Astron. Astrophys.* **478**, 897 – 906. doi:10.1051/0004-6361:20078615.

Biesecker, D.A., Myers, D.C., Thompson, B.J., Hammer, D.M., Vourlidas, A.: 2002, Solar phenomena associated with "EIT waves". *Astrophys. J.* **569**, 1009 – 1015. doi:10.1086/339402.

Chen, P.F.: 2009, The relation between EIT waves and coronal mass ejections. *Astrophys. J. Lett.* **698**, L112 – L115. doi:10.1088/0004-637X/698/2/L112.

Chertok, I.M.: 2006, Large-scale activity in major solar eruptive events of November 2004 according to SOHO data. *Astron. Rep.* **50**, 68 – 78. doi:10.1134/S1063772906010082.

Chertok, I.M., Grechnev, V.V.: 2003, Large-scale dimmings produced by solar coronal mass ejections according to SOHO/EIT data in four EUV lines. *Astron. Rep.* **47**, 934 – 945. doi:10.1134/1.1626196.

Chertok, I.M., Grechnev, V.V.: 2005, Large-scale activity in the Bastille day 2000 solar event. *Solar Phys.* **229**, 95 – 114. doi:10.1007/s11207-005-3654-1.

Cliver, E.W., Laurenza, M., Storini, M., Thompson, B.J.: 2005, On the origins of solar EIT waves. *Astrophys. J.* **631**, 604 – 611. doi:10.1086/432250.

Cohen, O., Attrill, G.D.R., Manchester, W.B., Wills-Davey, M.J.: 2009, Numerical simulation of an EUV coronal wave based on the 2009 February 13 CME event observed by STEREO. *Astrophys. J.* **705**, 587 – 602. doi:10.1088/0004-637X/705/1/587.

Culhane, J.L., Harra, L.K., James, A.M., Al-Janabi, K., Bradley, L.J., Chaudry, R.A., Rees, K., Tandy, J.A., Thomas, P., Whillock, M.C.R., Winter, B., Doschek, G.A., Korendyke, C.M., Brown, C.M., Myers, S., Mariska, J., Seely, J., Lang, J., Kent, B.J., Shaughnessy, B.M., Young, P.R., Simnett, G.M., Castelli, C.M., Mahmoud, S., Mapson-Menard, H., Probyn, B.J., Thomas, R.J., Davila, J., Dere, K., Windt, D., Shea, J., Hagood, R., Moye, R., Hara, H., Watanabe, T., Matsuzaki, K., Kosugi, T., Hansteen, V., Wikstol, Ø.: 2007, The EUV imaging spectrometer for *Hinode*. *Solar Phys.* **243**, 19 – 61. doi:10.1007/s01007-007-0293-1.

Delaboudinière, J.P., Artzner, G.E., Brunaud, J., Gabriel, A.H., Hochedez, J.F., Millier, F., Song, X.Y., Au, B., Dere, K.P., Howard, R.A., Kreplin, R., Michels, D.J., Moses, J.D., Defise, J.M., Jamar, C., Rochus, P., Chauvineau, J.P., Marioge, J.P., Catura, R.C., Lemen, J.R., Shing, L., Stern, R.A., Gurman, J.B., Neupert, W.M., Maucherat, A., Clette, F., Cugnon, P., van Dessel, E.L.: 1995, EIT: Extreme-ultraviolet imaging telescope for the SOHO mission. *Solar Phys.* **162**, 291 – 312. doi:10.1007/BF00733432.

Delannée, C., Hochedez, J.F., Aulanier, G.: 2007, Stationary parts of an EIT and moreton wave: a topological model. *Astron. Astrophys.* **465**, 603 – 612. doi:10.1051/0004-6361:20065845.

Domingo, V., Fleck, B., Poland, A.I.: 1995, The SOHO mission: an overview. *Solar Phys.* **162**, 1 – 37. doi:10.1007/BF00733425.

Doschek, G.A., Warren, H.P., Mariska, J.T., Muglach, K., Culhane, J.L., Hara, H., Watanabe, T.: 2008, Flows and nonthermal velocities in solar active regions observed with the EUV imaging spectrometer on *Hinode*: a tracer of active region sources of heliospheric magnetic fields? *Astrophys. J.* **686**, 1362 – 1371. doi:10.1086/591724.

Freeland, S.L., Handy, B.N.: 1998, Data analysis with the SolarSoft system. *Solar Phys.* **182**, 497 – 500.

Golub, L., Deluca, E., Austin, G., Bookbinder, J., Caldwell, D., Cheimets, P., Cirtain, J., Cosmo, M., Reid, P., Sette, A., Weber, M., Sakao, T., Kano, R., Shibasaki, K., Hara, H., Tsuneta, S., Kumagai, K., Tamura, T., Shimojo, M., McCracken, J., Carpenter, J., Haight, H., Siler, R., Wright, E., Tucker, J., Rutledge, H., Barbera, M., Peres, G., Varisco, S.: 2007, The X-ray telescope (XRT) for the *Hinode* mission. *Solar Phys.* **243**, 63 – 86. doi:10.1007/s11207-007-0182-1.

Harra, L.K., Sterling, A.C.: 2001, Material outflows from coronal intensity "Dimming Regions" during coronal mass ejection onset. *Astrophys. J. Lett.* **561**, L215 – L218. doi:10.1086/324767.

Harra, L.K., Hara, H., Imada, S., Young, P., Williams, D.R., Sterling, A.C., Korendyke, C., Attrill, G.D.R.: 2007, Coronal dimmings observed with *Hinode*: outflows related to a coronal mass ejection. *Publ. Astron. Soc. Japan* **59**, S801 – S806.

Harra, L.K., Sakao, T., Mandrini, C.H., Hara, H., Imada, S., Young, P.R., van Driel-Gesztelyi, L., Baker, D.: 2008, Outflows at the edges of active regions: contribution to solar wind formation? *Astrophys. J. Lett.* **676**, L147 – L150. doi:10.1086/587485.

Harra, L.K., Williams, D.R., Wallace, A.J., Magara, T., Hara, H., Tsuneta, S., Sterling, A.C., Doschek, G.A.: 2009, Coronal nonthermal velocity following helicity injection before an X-class flare. *Astrophys. J. Lett.* **691**, L99 – L102. doi:10.1088/0004-637X/691/2/L99.

Harrison, R.A., Lyons, M.: 2000, A spectroscopic study of coronal dimming associated with a coronal mass ejection. *Astron. Astrophys.* **358**, 1097 – 1108.

Hudson, H.S., Cliver, E.W.: 2001, Observing coronal mass ejections without coronagraphs. *J. Geophys. Res.* **106**, 25199 – 25214. doi:10.1029/2000JA004026.

Hudson, H.S., Webb, D.F.: 1997, Soft X-ray signatures of coronal ejections. *AGU Monograph*.

Hudson, H.S., Acton, L.W., Freeland, S.L.: 1996, A long-duration solar flare with mass ejection and global consequences. *Astrophys. J.* **470**, 629 – 635. doi:10.1086/177894.

Imada, S., Hara, H., Watanabe, T., Asai, A., Kamio, S., Matsuzaki, K., Harra, L.K., Mariska, J.T.: 2007, Discovery of the temperature-dependent upflow in the plage region during the gradual phase of the X-class flare. *Publ. Astron. Soc. Japan* **59**, S793 – S799.

Jin, M., Ding, M.D., Chen, P.F., Fang, C., Imada, S.: 2009, Coronal mass ejection induced outflows observed with *Hinode*/EIS. *Astrophys. J.* **702**, 27 – 38. doi:10.1088/0004-637X/702/1/27.

Kahler, S.W., Hudson, H.S.: 2001, Origin and development of transient coronal holes. *J. Geophys. Res.* **106**, 29239 – 29248. doi:10.1029/2001JA000127.

Ko, Y., Raymond, J.C., Zurbuchen, T.H., Riley, P., Raines, J.M., Strachan, L.: 2006, Abundance variation at the vicinity of an active region and the coronal origin of the slow solar wind. *Astrophys. J.* **646**, 1275 – 1287. doi:10.1086/505021.

Kojima, M., Fujiki, K., Ohmi, T., Tokumaru, M., Yokobe, A., Hakamada, K.: 1999, Low-speed solar wind from the vicinity of solar active regions. *J. Geophys. Res.* **104**, 16993 – 17004. doi:10.1029/1999JA900177.

Kosugi, T., Matsuzaki, K., Sakao, T., Shimizu, T., Sone, Y., Tachikawa, S., Hashimoto, T., Minesugi, K., Ohnishi, A., Yamada, T., Tsuneta, S., Hara, H., Ichimoto, K., Suematsu, Y., Shimojo, M., Watanabe, T., Shimada, S., Davis, J.M., Hill, L.D., Owens, J.K., Title, A.M., Culhane, J.L., Harra, L.K., Doschek, G.A., Golub, L.: 2007, The *Hinode* (Solar-B) mission: an overview. *Solar Phys.* **243**, 3 – 17. doi:10.1007/s11207-007-9014-6.

Kubo, M., Yokoyama, T., Katsukawa, Y., Lites, B., Tsuneta, S., Suematsu, Y., Ichimoto, K., Shimizu, T., Nagata, S., Tarbell, T.D., Shine, R.A., Title, A.M., Elmore, D.: 2007, *Hinode* observations of a vector magnetic field change associated with a flare on 2006 December 13. *Publ. Astron. Soc. Japan* **59**, S779 – S784.

Landau, L.D., Lifshitz, E.M.: 1987, *Fluid Mechanics, Course of Theoretical Physics, Vol. 6*, 2nd edn., Elsevier, New York.

Ma, S., Attrill, G.R.R., Golub, L., Lin, J.: 2010, Statistical study of CMEs with and without distinct low coronal signatures. *Astrophys. J.*, submitted.

Mandrini, C.H., Pohjolainen, S., Dasso, S., Green, L.M., Démoulin, P., van Driel-Gesztelyi, L., Copperwheat, C., Foley, C.: 2005, Interplanetary flux rope ejected from an X-ray bright point. The smallest magnetic cloud source-region ever observed. *Astron. Astrophys.* **434**, 725 – 740. doi:10.1051/0004-6361:20041079.

Mandrini, C.H., Nakwacki, M.S., Attrill, G., van Driel-Gesztelyi, L., Démoulin, P., Dasso, S., Elliott, H.: 2007, Are CME-related dimmings always a simple signature of interplanetary magnetic cloud footpoints? *Solar Phys.* **244**, 25 – 43. doi:10.1007/s11207-007-9020-8.

McIntosh, S.W.: 2009, The inconvenient truth about coronal dimmings. *Astrophys. J.* **693**, 1306 – 1309. doi:10.1088/0004-637X/693/2/1306.

McIntosh, S.W., Leamon, R.J., Davey, A.R., Wills-Davey, M.J.: 2007, The posteruptive evolution of a coronal dimming. *Astrophys. J.* **660**, 1653 – 1659. doi:10.1086/512665.

Noci, G.: 1973, Energy budget in coronal holes. *Solar Phys.* **28**, 403 – 407. doi:10.1007/BF00152311.

Odstrcil, D., Pizzo, V.J., Arge, C.N.: 2005, Propagation of the 12 May 1997 interplanetary coronal mass ejection in evolving solar wind structures. *J. Geophys. Res.* **110**, A02106. doi:10.1029/2004JA010745.

Podladchikova, O., Berghmans, D.: 2005, Automated detection of EIT waves and dimmings. *Solar Phys.* **228**, 265 – 284. doi:10.1007/s11207-005-5373-z.

Reinard, A.A., Biesecker, D.A.: 2008, Coronal mass ejection-associated coronal dimmings. *Astrophys. J.* **674**, 576 – 585. doi:10.1086/525269.

Robbrecht, E., Patsourakos, S., Vourlidas, A.: 2009, No trace left behind: STEREO observation of a coronal mass ejection without low coronal signatures. *Astrophys. J.* **701**, 283 – 291. doi:10.1088/0004-637X/701/1/283.

Rust, D.M.: 1983, Coronal disturbances and their terrestrial effects, tutorial lecture. *Space Sci. Rev.* **34**, 21 – 36.

Rust, D.M., Hildner, E.: 1976, Expansion of an X-ray coronal arch into the outer corona. *Solar Phys.* **48**, 381 – 387.

Sakao, T., Kano, R., Narukage, N., Kotoku, J., Bando, T., DeLuca, E.E., Lundquist, L.L., Tsuneta, S., Harra, L.K., Katsukawa, Y., Kubo, M., Hara, H., Matsuzaki, K., Shimojo, M., Bookbinder, J.A., Golub, L., Korreck, K.E., Su, Y., Shibasaki, K., Shimizu, T., Nakatani, I.: 2007, Continuous Plasma Outflows from the edge of a solar active region as a possible source of solar wind. *Science* **318**, 1585 – 1588. doi:10.1126/science.1147292.

Schrijver, C.J., De Rosa, M.L., Metcalf, T., Barnes, G., Lites, B., Tarbell, T., McTiernan, J., Valori, G., Wiegelmann, T., Wheatland, M.S., Amari, T., Aulanier, G., Démoulin, P., Fuhrmann, M., Kusano, K., Régnier, S., Thalmann, J.K.: 2008, Nonlinear force-free field modeling of a solar active region around the time of a major flare and coronal mass ejection. *Astrophys. J.* **675**, 1637 – 1644. doi:10.1086/527413.

Sterling, A.C., Hudson, H.S.: 1997, YOHKOH SXT observations of X-ray "Dimming" associated with a Halo coronal mass ejection. *Astrophys. J. Lett.* **491**, L55 – L58. doi:10.1086/311043.

Thompson, B.J., Plunkett, S.P., Gurman, J.B., Newmark, J.S., St. Cyr, O.C., Michels, D.J.: 1998, SOHO/EIT observations of an Earth-directed coronal mass ejection on May 12, 1997. *Geophys. Res. Lett.* **25**, 2465 – 2468. doi:10.1029/98GL50429.

Thompson, B.J., Cliver, E.W., Nitta, N., Delannée, C., Delaboudinière, J.P.: 2000, Coronal dimmings and energetic CMEs in April – May 1998. *Geophys. Res. Lett.* **27**, 1431 – 1434. doi:10.1029/1999GL003668.

Tsuneta, S., Acton, L., Bruner, M., Lemen, J., Brown, W., Caravalho, R., Catura, R., Freeland, S., Jurcevich, B., Owens, J.: 1991, The soft X-ray telescope for the SOLAR-A mission. *Solar Phys.* **136**, 37 – 67.

van Driel-Gesztelyi, L., Attrill, G.D.R., Démoulin, P., Mandrini, C.H., Harra, L.K.: 2008, Why are CMEs large-scale coronal events: nature or nurture? *Ann. Geophys.* **26**, 3077 – 3088.

Veronig, A.M., Temmer, M., Vršnak, B.: 2008, High-cadence observations of a global coronal wave by STEREO EUVI. *Astrophys. J. Lett.* **681**, L113 – L116. doi:10.1086/590493.

Vršnak, B., Cliver, E.W.: 2008, Origin of coronal shock waves. Invited review. *Solar Phys.* **253**, 215 – 235. doi:10.1007/s11207-008-9241-5.

Wang, T., Yan, Y., Wang, J., Kurokawa, H., Shibata, K.: 2002, The large-scale coronal field structure and source region features for a Halo coronal mass ejection. *Astrophys. J.* **572**, 580 – 597. doi:10.1086/340189.

Warmuth, A.: 2007, Large-scale waves and shocks in the solar corona. In: Klein, K.L., MacKinnon, A.L. (eds.) *Lecture Notes in Physics*, **725**, Springer, Berlin, 107 – 138.

Webb, D.F., Lepping, R.P., Burlaga, L.F., DeForest, C.E., Larson, D.E., Martin, S.F., Plunkett, S.P., Rust, D.M.: 2000, The origin and development of the May 1997 magnetic cloud. *J. Geophys. Res.* **105**, 27251 – 27260. doi:10.1029/2000JA000021.

Williams, D.R., Harra, L.K., Brooks, D.H., Imada, S., Hansteen, V.H.: 2009, Evidence from the extreme-ultraviolet imaging spectrometer for axial filament rotation before a large flare. *Publ. Astron. Soc. Japan* **61**, 493 – 497.

Wills-Davey, M.J., Attrill, G.D.R.: 2010, EIT waves: a changing understanding over a solar cycle. *Space Sci. Rev.*, 325 – 353. doi:10.1007/s11214-009-9612-8.

Wu, S.T., Zheng, H., Wang, S., Thompson, B.J., Plunkett, S.P., Zhao, X.P., Dryer, M.: 2001, Three-dimensional numerical simulation of MHD waves observed by the extreme ultraviolet imaging telescope. *J. Geophys. Res.* **106**, 25089 – 25102. doi:10.1029/2000JA000447.

Yashiro, S., Gopalswamy, N., Michalek, G., St. Cyr, O.C., Plunkett, S.P., Rich, N.B., Howard, R.A.: 2004, A catalog of white light coronal mass ejections observed by the SOHO spacecraft. *J. Geophys. Res.* **109**, 7105. doi:10.1029/2003JA010282.

Zhukov, A.N., Auchère, F.: 2004, On the nature of EIT waves, EUV dimmings and their link to CMEs. *Astron. Astrophys.* **427**, 705 – 716. doi:10.1051/0004-6361:20040351.